Dissecting the role of lipid metabolism and the nature of autophagosomal cargo in Central Nervous System

Master Thesis

Garyfallia Gouna, BSc

Committee
Vassiliki Nikoletopoulou, PhD
Ioannis Zaganas, PhD, MD
Dimitris Kardassis, PhD

November, 20th, 2018, Heraklion, Greece

Dissecting the role of lipid metabolism and the nature of autophagosomal cargo in the Central Nervous System

Garyfallia Gouna [1,2]

[1]Institute of Molecular Biology and Biotechnology, Foundation for Research and Technology – Hellas, Nikolaou Plastira 100, Heraklion 70013, Crete, Greece, [2]School of Medicine, University of Crete, Heraklion, Greece

Abstract

Lipids represent key macromolecules of vital importance for the maintenance of brain homeostasis, from a structural and a signaling point of view. Lipid droplets (LDs), the storage organelles of the lipids, are selectively degraded by macroautophagy in several tissues, a process known as lipophagy. There is a growing body of literature, suggesting that lipophagy provides the platform for utilization of lipids not only as energy resources, but also as signaling molecules. However, the role of lipophagy in the central nervous system (CNS) is poorly understood. Here, we try to address if lipophagy regulates the mobilization of lipids in neurons, by monitoring two LD protein markers, RAB18 and PLIN2. We report that, RAB18 appears to be a positive modulator of autophagy, whereas PLIN2 protein acts as an autophagic substrate. The absence of colocalization of RAB18 and PLIN2 suggest the existence of two distinct LD populations with potential diverse functions. This hypothesis is further supported by the different localization of these two markers on the autophagosome. Interestingly, there is strong evidence of RAB18 localization in the ER and nuclei compartments in CNS, while mounting evidence support a positive association of RAB18 and autophagosomal biogenesis. In addition, synaptic

and cytoskeletal proteins were primarily identified as autophagic cargo from the forebrain of young and mature animals, by conducting Tandem Mass Spectrometry proteomic analyses. Thus, the association of autophagy to synaptic and cytoskeletal functions is highlighted. Overall, our findings emphasize the presence of distinct LD populations in neurons, which are regulated via the lipophagy mechanism, and may maintain synaptic homeostasis. To our knowledge, this is the first study indicating that RAB18 and PLIN2 associate with lipophagy in CNS. Last, this study draws the initial route of characterizing the autophagic cargo of forebrain amongst young and mature animals, providing important evidence for autophagy's role across maturation in the brain.

Διερεύνηση του μεταβολισμού των λιπιδίων και της φύσης του αυτοφαγικού φορτίου στο Κεντρικό Νευρικό Σύστημα

Γαρυφαλλιά Γούνα [1,2]

[1]Institute of Molecular Biology and Biotechnology, Foundation for Research and Technology – Hellas, Nikolaou Plastira 100, Heraklion 70013, Crete, Greece, [2]School of Medicine, University of Crete, Heraklion, Greece

Περίληψη

Τα λιπίδια αντιπροσωπεύουν βασικά μακρομόρια ζωτικής σημασίας για τη διατήρηση της ομοιόστασης του εγκεφάλου, από δομική και σηματοδοτική άποψη. Τα σταγονίδια λιπιδίων (LDs), τα οργανίδια αποθήκευσης των λιπιδίων, αποικοδομούνται επιλεκτικά με μακροαυτοφαγία σε αρκετούς ιστούς, μια διαδικασία γνωστή ως λιποφαγία. Ένα ολοένα αυξανόμενο σώμα βιβλιογραφίας υποδηλώνει ότι η λιποφαγία συμμετέχει στη κινητοποίηση των λιπιδίων, τα οποία δρουν στα κύτταρα ως μόρια σηματοδότησης και ως ενεργειακοί πόροι. Ωστόσο, ο ρόλος της λιποφαγίας στο κεντρικό νευρικό σύστημα (ΚΝΣ) είναι ελάχιστα κατανοητός. Στη συγκεκριμένη διπλωματική εργασία διερευνούμε εάν η λιποφαγία ρυθμίζει την κινητοποίηση λιπιδίων στους νευρώνες, παρακολουθώντας δύο πρωτεϊνικούς δείκτες των LD, τους RAB18 και PLIN2. Αναφέρουμε ότι η RAB18 πρωτεΐνη φαίνεται να είναι ένας θετικός διαμορφωτής της αυτοφαγίας, ενώ η πρωτεΐνη PLIN2 δρα ως αυτοφαγικό υπόστρωμα. Η απουσία συνεντόπισης των RAB18 και PLIN2 υποδηλώνει την ύπαρξη δύο ξεχωριστών LD πληθυσμών με πιθανές διαφορετικές λειτουργίες. Αυτή η υπόθεση υποστηρίζεται περαιτέρω από τον διαφορετικό εντοπισμό αυτών των δύο δεικτών στο αυτοφαγόσωμα. Είναι ενδιαφέρον ότι

υπάρχουν ισχυρές ενδείξεις για τον εντοπισμό του RAB18 στο ενδοπλασματικό δίκτυο (ER) και στους πυρήνες στο ΚΝΣ, ενώ τα αυξανόμενα στοιχεία υποστηρίζουν μια θετική συσχέτιση του RAB18 και της βιογένεσης των αυτοφαγωσωμάτων. Επιπλέον, συναπτικές και κυτταροσκελετικές πρωτεΐνες προσδιορίστηκαν ως ένα από τα κύρια αυτοφαγικά φορτία από τον πρόσθιο εγκέφαλο των νεαρών και ώριμων ζώων, με τη διεξαγωγή αναλυτικών πρωτεϊνικών αναλύσεων Tandem Mass Spectrometry. Με τον τρόπο αυτό,τονίζεται η συσχέτιση της αυτοφαγίας με τις συναπτικές και κυτταροσκελετικές λειτουργίες του εγκεφάλου. Συνολικά, τα ευρήματά μας υπογραμμίζουν την παρουσία ξεχωριστών LD πληθυσμών σε νευρώνες, οι οποίοι ρυθμίζονται μέσω του μηχανισμού λιποφαγίας και μπορεί να διατηρούν τη συναπτική ομοιόσταση. Μέχρι τώρα, αυτή είναι η πρώτη μελέτη που δείχνει ότι οι RAB18 και PLIN2 πρωτεΐνες σχετίζονται με τη λιποφαγία στο ΚΝΣ. Τέλος, η μελέτη αυτή χαρακτηρίζει σε έναν αρχικό βαθμό το αυτοφαγικό φορτίο του πρόσθιου εγκεφάλου μεταξύ των νεαρών και ώριμων ζώων, παρέχοντας σημαντικά στοιχεία για τον ρόλο της αυτοφαγίας στην ωρίμανση του εγκεφάλου.

Table of Contents

Acknowledgements

This thesis was funded by the ERC Starting Grant 2016: "The role of autophagy in Synaptic Plasticity–NEUROPHAGY". I would like to sincerely express my gratitude to my supervisor, Dr. Vassiliki Nikoletopoulou, who gave me the opportunity to study a personal idea and for her constructive and valuable leadership throughout the project. I really admire her passion and commitment to research, a characteristic that is transmitted to colleagues in the lab. Also, I would like to thank Prof. Ioannis Zaganas and Prof. Dimitris Kardassis for their help and support all of these years.

In addition, I am grateful that I had the chance to get to know and work with amazing colleagues: Emmanouela Kallergi, Akrivi-Dimitra Daskalaki, Christianne Halder, Theodora Chalatsi, Anastasios Kollias, Aggeliki Swthriou, Angeliki Kolaxi, Eva Ioannou, Ioanna Zwta and all the people that rotated to our lab. Our everyday collaboration and brain storming boosted the project and I can say with safety that we have become good friends. I hope in the future our professional and personal routes will be common once more.

Moreover, I would like to thank from the bottom of my heart my family, my father Panagiotis, my mother Stavroula and my brother Nikos, for their encouragement and assistance all of these years. They are the reason for what I have become in this society. And...last but surely not least, I would like to truly thank Dr. Spyridon Chavlis, my personal guide and companion the last three and a half years. Without his guidance, support and loyalty, I would not have gone far in the research arena.

Introduction

The characterization of AuTophaGy-related gene family (Atg)[1] in *Saccharomyces cerevisiae*, illuminated and acknowledge a field initiated by Christian de Duve, who introduced the term of autophagy as a vital part of maintaining cellular homeostasis[2,3]. Autophagy (from the Greek word αυτοφαγία, meaning "eat yourself"), is a major degradative process, which primary goal is to deliver cytoplasmic entities to the final destination, the lysosomes. Autophagy is a broad definition, which comprises of three autophagic subtypes[4]. Chaperon-mediated autophagy (CMA) mediates the transport of intracellular proteins, targeted to their specific motif "KFERQ" by heat shock cognate 71 kDa protein (HSPA8) chaperone[5], directly to lysosomes[6]. It has been documented that CMA does not participate to the catabolism of lipids or other molecular compounds, but targets only soluble proteins[7]. Microautophagy includes the immediate engulfment of cytoplasmic material by the lysosome (mammals) or vacuole (yeast and plants), via invagination of their membranes[8]. This kind of autophagy also contributes to the degradation of organelles, including lipid droplets[9,10] and mitochondria[11], while recently a cross-talk between CMA and microautophagy was reviewed in extent[12].

The third and most well characterized autophagy variant is macroautophagy (hereafter termed as autophagy), the only subtype that recruits a double-membrane organelle, the autophagosome (AV), destined for targeting intracellular content to the lysosome[13]. It is strongly believed that, the AV formation initiate to the endoplasmatic reticulum (ER)[14], although nearly every subcellular compartment contributes to this process[15]. More specifically, in response to amino acid scarcity, the mammalian target of rapamycin (mTOR) is inactivated. Following this event,

the isolation membrane or phagophore is formed when a serine-threonine kinase complex (ULK complex) assemblies and translocates to a specific ER location, marked by autophagy-related protein 9A (ATG9A)[16]. . Phagophore initiation takes place in a structure, positively stained for zinc finger FYVE-type containing 1 (ZFYVE1 or DFCP1), the omegasome[14]. ULK complex includes unc-51-like autophagy activating kinase 1&2 (ULK1, ULK2), RB1 inducible coiled-coil 1 (RB1CC1 or FIP200), autophagy-related protein 13 (ATG13) and autophagy-related protein 101 (ATG101). These four proteins represent the pre-autophagosomal structure (PAS) components, core machinery for the biogenesis of the phagophore. Both FIP200 and ATG13 are essential for the localization and stability of ULK1 to the phagophore[17]. ULK1 is further stabilized to the PAS complex by the assistance of ATG13-binding protein, ATG101[18,19]. Concomitantly, ULK1 phosphorylates ATG9A[20], an event that promotes the expansion of the isolation membrane, by incorporating phospholipids from several sources, such as mitochondria, ER and recycling endosomes[21]. In parallel, a group of proteins belonging to class III phosphatidylinositol 3-kinase (PtdIns3-kinase – PI3K) family are recruited with the ultimate purpose of the expansion of the isolation membrane. This family consists of beclin 1 (BECN1), phosphatidylinositol 3-kinase catalytic subunit type 3 (PIK3C3 or VPS34) and beclin 1-associated autophagy-related key regulator (ATG14L), among others. ATG14L associates with BECN1[22], a fundamental subunit of PI3K complex that promotes the formation of phosphatidylinositol 3-phosphate (PtdIns3P or PI3P)[23]. Simultaneously, activated VPS34 also produces PI3P, leading to further elongation of the phagophore[24], while members of the human WD-repeat protein interacting with phosphoinositides (WIPI) family have been characterized as important PI3P-binding effectors, autophagy-specific[25]. The two main ubiquitination-like events that promote the elongation of the autophagosomal membrane include the conjugation of Atg12

to Atg5 by Atg7 (resembling E1 ubiquitin-activating enzyme) and Atg10 (resembling E2 ubiquitin-conjugating enzyme). The Atg12-Atg5 complex associates with Atg16L1, and this three-member complex binds to the isolation membrane[26]. Additionally, members of the mammalian Atg8 family (MAP1LC3 or LC3- microtubule-associated protein light chain 3, GABARAP - γ-aminobutyric acid receptor-associated protein) are conjugated to phosphatidylethanolamine (PE). LC3, the best characterized member, conjugates to PE via Atg7 and Atg3, resulting in the lipidated form of LC3, LC3-II. In this conformation, LC3-II becomes an integral part of both membranes of the AV and remains intact after the AV-lysosomal or AV-endosomal fusion, to create the autolysosome of amphisome, respectively[26]. The closed, mature AV fuses with the lysosome, by incorporating its outer membrane to the lysosomal single membrane. The delivered cargo, along with the inner autophagosomal membrane, is degraded by lysosomal hydrolases, while LC3-II of the outer autophagosomal membrane is de-lipidated and recycled back to the cytoplasm. The AV-lysosome fusion depends on a great variety of cytoskeletal proteins, phospholipids and SNARE complexes[13].

Since autophagy acts as a homeostatic mechanism for the cell, it is anticipated to be strictly regulated. The main negative regulator of autophagy is mTOR[27]. Precisely, under amino acid supply, the lysosomal vacuolar-type H+-translocating ATPase, conjugated with Ragulator complex and RRAG proteins, target the mammalian target of rapamycin complex 1 (mTORC1) to the lysosomal membrane[28], where it is activated by RHEB GTPase[29]. Activated mTOR inhibits ULK1, through phosphorylation[30]. Moreover, glucose supply can modulate autophagy, as activated protein kinase A (PKA) inhibits AMP-activated protein kinase (AMPK)[31], a key inhibitor of mTORC1. AMPK phosphorylates the mTORC1 subunit RPTOR/raptor and the

tuberous sclerosis proteins 2 (TSC2), both of which result in attenuation of mTORC1[32]. AMPK also promotes autophagic responses, as activates ULK1 by phosphorylation[30]. Apart from post-translational regulatory mechanisms, autophagy is regulated in the transcriptional level as well. Inactivation of mTORC1 results in the translocation of the unphosphorylated transcription factor EB (TFEB) from the cytoplasm to the nucleus, where it mediates the transcription of several genes, responsible for autophagic machinery and the biogenesis of lysosome[33]. Furthermore, lipid metabolism contributes to autophagy regulation. Excessive amount of lipids are described to block autophagy, by inhibiting AV-lysosome fusion, or disrupting the function of lysosomal hydrolases or lysosome acidification[34,35]. On the contrary, free fatty acids (FFA), for example oleic acid, an unsaturated fatty acid, inhibit mTORC1 or implicate the PKR–JNK (RNA-dependent protein kinase- c-Jun N-terminal kinase) pathway, thus increasing autophagy[36,37]. Though autophagy was thought to represent a bulk catabolic machinery, a growing body of literature support the selectivity of this process, highlighting the presence of selective autophagy receptors (SARs) that directly target intracellular contents for degradation[38] and the role of cargo morphology to its own recognition by AVs[39]. For example, sequestosome-1 (SQSTM1 or ubiquitin-binding protein p62) and autophagy-linked FYVE protein (ALFY) represent two of the best described autophagic receptors, which intercede the degradation of ubiqutinated cargos[40,41]. The characterization of the LC3 interacting region (LIR) motif, a core consensus sequence of [W/F/Y]xx[L/I/V], present in the protein sequence of several cargoes, pioneered the field of selective autophagy[42]. In general, apart from intracellular proteins, autophagic substrates can consist of bacteria, (xenophagy), viruses (virophagy), lipid droplets (lipophagy), aggregates (aggrephagy), mitochondria (mitophagy), peroxisomes (pexophagy), ribosomes (ribophagy), nucleus (nucleophagy), ER (reticulophagy), inactive proteasomes (proteophagy) and lysosomes

(lysophagy)[4,43]. Autophagic cargo is of great significance, since its degradation maintains the basal cellular homeostasis. Presently, with the development of new mass spectrometry techniques, the proteome of autophagic structures begins to be elucidated. A variety of studies focus on whole cell proteomes from diseased cells and model organisms, whereas others target the contents of specific organelles, as autophagosomes and lysosomes under physiological conditions from several cell and tissue types. What's more, secretome proteomics consist an emerging research field[44]. It is widely held view that proteomic and lipidomic analyses pioneer our understanding of autophagic machinery, since the engulfed cargo is directly identified in numerous healthy or pathological circumstances.

Lipophagy describes the selective autophagic process of neutral lipid droplets (LDs), thus promoting release of fatty acids to the cytosol. In a next step, fatty acids undergo β-oxidation in mitochondria for energy requirements[45,46]. Actually, macrolipophagy (hereafter refer to as lipophagy), the selective sequestration of LDs by macroautophagy, was the initial description of lipophagy, introduced to the field by Singh, Kaushik and colleagues on 2009. Specifically, it was identified that, either pharmacological or genetic inhibition of autophagy in hepatocytes promotes the storage of TG into LDs. Extensive electron microscopy showed that LDs are delivered to lysosomes via AVs, while LDs and AVs association was prominent during nutrient scarcity in vivo[47]. Nowadays, LDs are considered as extremely dynamic organelles, with high regulatory aspects, and a complete different spatial organization, size and number, within and between distinct cell types. LDs morphology includes a hydrophobic lipid core of triglycerides (TG), sterol esters (SE) and retinyl esters (RE). TG are composed by two pathways, the monoacylglycerol and glycerol phosphate pathways, whereas SE are the final molecules of sterol

ester synthesis pathway[48]. RE are composed by the esterification of the C-terminus of retinol[49]. The synthesis of TG, SE and RE is the first step of LDs biogenesis, which occurs in a specialized structure of the endoplasmatic reticulum (ER) bilayer, the lens. Ultimately, following this accumulation, an initial LD (iLD) is created and buds from the ER bilayer. iLD can reconnect to the ER, when its surface tension is increased, an event provoked by coat protein complexes I (COPI). This connection allows for various, ER originated, proteins, to tether and facilitate LD expansion (eLD), due to TG synthesis[50]. LD hydrophobic core is surrounded by a phospholipid monolayer, where several proteins are tethered. These proteins, originated from the ER bilayer (Class I) or the cytosol (Class II), attach to LD surface by lipid-anchors, hairpin or amphipatic helices[51,52]. Although the majority of literature strongly supports the ER as the LDs biogenesis site, a recent study offers proof of a nuclear LD formation (nLD) in hepatic cell lines and primary hepatocytes[53]. Intriguingly, LDs core material (TG and SE) aids to the formation of PAS after fasting-induced autophagy[54], elucidating the crucial importance of lipids in the autophagosomal membrane, a poorly understood field[55].

There is a plethora of identified proteins, that coat LD surface[56]. Of particular interest, Ras-related protein Rab-18 (RAB18) and perilipin-2 (PLIN2) proteins are localized to LD surface and are ubiquitously expressed in all cells. RAB18 and PLIN2 simultaneous expression has been studied in HepG2 cells, where their intensities appeared to be reciprocal. However, the overexpressed RAB18 (EGFP-RAB18) and PLIN2 showed hardly any overlapping, suggesting of the possible existence of two different LD populations[57]. RAB18 belongs to the small-GTPases family, and cycles between two conformations, the inactive GDP-bound and the active GTP-bound form. It is known that guanine nucleotide exchange factors (GEFs) mediate the

exchange of GDP to GTP, stimulating the binding of small-GTPases to their target membranes[58]. To our knowledge, two proteins have been suggested to act as GEFs for RAB18, Rab3GAP (Rab3 GTPase-activating protein) complex[59] and TRAPPII (trafficking protein particle complex II)[60]. Interestingly, both studies describe an association of RAB18 and ER, with Rab3GAP complex to be essential for the direct tethering of RAB18 to ER, while COPI-TRAPPII association in the ER, facilitates the direct binding of RAB18 to LDs, which in turn mediates an ER-LD communication bridge. RAB18 role in ER-LD contact sites is further supported in a recent study, where LD-tethered RAB18 bounds exclusively to ER associated NAG-RINT1-ZW10 (NRZ) tethering complex, which in turn is connected to ER-associated SNAREs (Syntaxin18, Use1, BNIP1)[61]. RAB18 exploits a lipid-anchor to attach to LD surface[62], and has been suggested to be an exclusive LD resident amongst all the characterized Rabs in several tissue and cell types[57,63,64]. RAB18 is documented to be a positive modulator of autophagy[65], while its GEF, RAB3GAP, also modulates basal autophagy[66]. Remarkably, according to a preliminary study, RAB18 is substantial for LD metabolism, as RAB18 knockout HeLa cells express diminished lipid disposal. This lipid scarcity provokes the translocation of ATG9A of the AV formation site, where it acts as a compensatory mechanism rescuing autophagic activity in basal, but not in autophagy induced conditions[67]. Still, in a human mammary cancerous cell line, RAB18 fail to provide evidence of participating in LD biogenesis of turnover[68]. RAB18 is observed inside the nucleus of a human liver cell line[53], further encourage the nuclear biogenesis of LDs.

PLIN2, a member of perilipin (PLIN) protein family with a PAT domain, consists one of the major LD residents[69] and is targeted to LD surface by amphipathic helices[70]. Particularly, PLIN2

is coated to LDs via COPI/COPII coatomer proteins and their respective regulators[71]. PLIN2 has a pivotal role in LD biogenesis, as the most prevalent theory of LD formation is their disassociation from PLIN2-enriched ER sites[72]. In addition, PLIN2 guards the LD structure, as it prevents adipose triglyceride lipase (ATGL) activity, while its deficiency results in the diminishing of LDs[73]. Interestingly, ATGL was found in the lipid droplet proteome[74], but recent evidence support that acts indirectly for the LD degradation, through the sirtuin-1 (SIRT1) dependent induction of lipophagy[75]. LD formation under the stimuli of oleic acid stabilizes PLIN2 amount on LD surface[76]. PLIN2 unbound form is located to the cytoplasm, where it is catabolized by the proteasome, via PLIN2 N-terminal acetylation, though it becomes stable while it locates on LDs[77,78]. Although LD-bound PLIN2 has been identified as a direct substrate of CMA[79], through its phosphorylation by AMPK[80], a recent study highlight PLIN2 role in modulating lipophagy in liver, where depletion of PLIN2 led to increased autophagy and diminished hepatic TG, while overexpression protected LD degradation via lipophagy[81].

Currently, it is widely accepted that lipids are fundamental components of the brain, where their concentration is the second highest in the human body, after adipose tissue. Lipids can be generally categorized in five classes: fatty acids (FA), TG, phospholipids, sphingolipids and sterol lipids. The brain fatty acids composition is consisting mostly of long-chain polyunsaturated fatty acids (LC-PUFAs), and a fraction of them are composed *de novo*, whereas vital FA are incorporated to neurons via crossing of blood brain barrier (BBB) from the systemic circulation[82]. In the brain, lipids are important as energy substrates, contradicting the notion that glucose holds the exclusivity of brain energy source. It has been demonstrated that fatty acid oxidation, which may occur only in astrocytes, represents almost 20% of the brain energy

source[83]. Besides, the most vital role of lipids in the brain is that they maintain the cellular membrane structure, a critical brain feature assisting in the compartmentalization of signaling processes. Cholesterol is such a lipid, which consists in all cellular membranes, is detrimental for membrane permeability and flexibility. Also, cholesterol appears to have a functional role in shaping lipid rafts, coming in close proximity with sphingolipids and phospholipids. Lipid rafts are seminal structures for organizing signaling molecules and mediate cytoskeletal changes, via the actin/tubulin remodeling, along with their trafficking and metabolic properties[84]. Likewise, lipids themselves function as bioactive molecules, affecting signaling procedures and controlling neurogenesis and cognition[85]. For example, TG turnover is mediated via ATGL and the end product is diacylglycerol (DAG). DAG, except for its precursor role for the phospholipid formation, can mediate various signaling processes[84], highlighting its importance in cellular crosstalk between the different brain regions. Hence, it is of particular essence that lipids portray a crucial role in various brain pathophysiologies, such as amyotrophic lateral sclerosis (ALS) and neurodegenerative diseases[86]. In fact, there is a growing body of literature depicts that ALS irritates lipid functionalities as energy substrates, components of cellular structures and modulators of signaling processes[84].

Lipophagy has been rarely studied in the brain. Actually, the first evidence of a possible lipophagic mechanism in the brain was provided on 2010. Striatal neurons from control animal of a Huntington's disease mouse model, depicted colocalization of AVs and LDs, after the attenuation of both AV-lysosome fusion and the lysosomal activity[87]. Another description of lipophagy was conducted in a hypothalamic neuronal cell line, where oleic/palmitic acid treatments provoke rapid induction of autophagy, in combination with the colocalization of AVs

and LDs, while silencing of *Atg5* gene results in lipid accumulation[88]. In a forced lipophagy model, LDs found to be essential for the early mouse development[89], an event that illustrates the importance of lipophagic machinery in brain development as well. In this thesis, we tried to determine the significance of lipid turnover in neurons, under numerous positive and negative autophagic triggers. Our particular interest lies on the identification of LDs, with the utility of two well characterized LD markers, RAB18 and PLIN2 proteins. On top of that, we set out to explore the autophagic cargo from isolated brain AVs, by conducting quantitative mass spectrometry proteomic analyses.

Materials and Methods

Mouse models

Animals protocols were authorized by the FORTH Animal Ethics Committee (FEC), while animals handling was performed by FELASA accreditated users. All mice were housed in a pathogen-free environment, in clear cages with stable room temperature (25 ^{o}C) and constant humidity in a 12 hr/12 hr light/dark cycle. All animals used were mice of C57BL/6 genetic background. As previously defined[90], conditional ablation of *Atg5* gene in the neural lineage (*cAtg5*) was succeeded when with Nestin-Cre mice were crossed with Atg5$^{f/f}$ mice (a generous gift of Dr. Aris Iliopoulos). Nestin-Cre mice were also crossed with BDNF$^{f/f}$ mice (a generous gift of Dr. Michael Sendtner), in order to obtain conditional knockout of *BDNF* gene in the neural lineage (*cBDNF*).

Starvation protocol

Adult (2 months old) male mice with a C57BL/6 genetic background were utilized for starvation experiments. For fasting, mice were deprived of all food for 24 hours, as indicated, with free access to water. Control mice were fed an *ad libitum* regime on chow (Mucedola, 4RF24 GLP). Neuronal cultures were fasted by the supply of plain Neurobasal medium (GIBCO, CTS 1X, without L-glutamine) for the indicative time periods.

Specific brain regions dissection

Brains, from indicative postnatal days age, were freshly isolated and dissected on ice to obtain cortex, hippocampus, hypothalamus and cerebellum, as previously described[91]. Subsequently, isolated brain regions were processed to obtain protein lysates. Otherwise, forebrain regions were immediately processed for AV or nuclei isolation.

Neuronal cultures

Mixed sex mouse embryos in embryonic day 15,5-16,5 (E15,5-E16,5) were dissected and the forebrain region was collected in filtered Phosphate Buffered Saline (PBS) 1X, pH=7,4 (NaCl 0.137 M, KCl 0.0027 M, Na_2HPO_4 0.01 M, KH_2PO_4 0.0018 M). After two centrifugations of 5min at 1000rpm, room temperature (RT), forebrains were treated with 0.25% trypsin in 37 ^oC, followed by chemical dissociation. Trypsin was inactivated by supply of DMEM/FBS (GIBCO, 1X Dulbecco's Modified Eagle Medium, 4.5g/L glucose / Fetal Bovine Serum). After one centrifugation of 5 min at 1000rpm, RT, dissociated neurons were plated at 12-well or 6-well plates, already coated with poly-D-lysine (Sigma-Aldrich) coverslips (12-well plate), and cultured in Neurobasal medium (GIBCO, CTS 1X, without L-glutamine), also containing L-glutamine (200 μM), penicillin (5 mg/ml), and streptomycin (12.5 mg/ml), B27 (2%) and β-mercaptoethanol (1%). The initial cell density was 250.000/cm^2, and nearly 1000000 and 3000000 neurons were plated in 12-well and 6-well plates respectively. After 6-23 days *in vitro* cells were treated with days in vitro, neurons were treated with BDNF (50ng/ml) and with the following inhibitors at the indicated final concentrations: Bafilomycin A1 (Sigma-Aldrich, 10nM), SBI- 0206965 (Sigma-Aldrich, 500nM). BDNF was submitted for 48 hours, while SBI

and Bafilomycin A1 (Baf A1) for 6 hours. Moreover, day *in vitro* 6 neurons were pulsed for 5 min with NMDA (50μM) and DHPG (50μM) and subsequently incubated for 2 hours with the remaining medium, before fixation, described in the immunostaining section. Oleic acid treatments (Sigma, 250μM) were performed in mature neurons. Oleic acid was diluted in BSA free fatty acid (Sigma, A6003). For oleic acid treatment, control neurons were treated with treated with BSA free fatty acid.

Immunostaining

Cultured neurons were washed with PBS 1X, pH=7,4 and fixed in 4% paraformaldehyde (PFA) in PBS. Consequently, 3 washes of PBS were performed and then cells were blocked for 1 hour at RT with blocking solution containing 10% FBS and 0,2% Triton-X in PBS. Neurons were subsequently incubated in primary antibody, diluted in blocking solution, for 24 hours at 4^{o}C. The following primary antibodies were utilized: LC3 (1:1000, mouse monoclonal, Santa Cruz, sc-376404 // 1:1000, rabbit affinity isolated, Sigma-Aldrich, L7543), p62 (1:5000, guinea pig polyclonal, PROGEN, GP62-C), MAP2 (1:2000, guinea pig polyclonal, Synaptic Systems, #188004), Neurofilament H (1:500, rabbit polyclonal, Synaptic Systems, #171102), RAB18 (1:1000, mouse monoclonal, Proteintech, 60057-1-Ig), PLIN2 (1:2000, rabbit polyclonal, Proteintech, 15294-1-AP), Alfy (1:1000, mouse monoclonal, Santa Cruz, sc-514569). After washes with PBS, neurons were incubated with secondary antibodies, diluted in PBS 1X, RT, for 1 hour avoiding light. The following secondary antibodies were used: anti-rabbit Alexa 488, anti-mouse Alexa 594, and anti-guinea pig Alexa 647, anti-rabbit Alexa 594, anti-mouse Alexa 488, and anti-rabbit Neurof 405. All Alexa (Abcam) antibodies were used in a final dilution of 1:1000, while Neurof in 1:100. Neurons nuclei were stained with the nuclear dye HOECHST

(1:5000), whereas neutral lipids were stained with the dye BODIPY 493/503 (1μg/ml working solution in PBS 1X or ddH_2O). Finally, neurons were washed with PBS 1X and mounted, with 80% glycerol in PBS 1X, onto slides. Confocal images of fluorescently labeled proteins were obtained using the Leica TSC SP8 inverted confocal microscope.

Immunohistochemistry

Fixation was performed in avertin (Sigma nominations) anaesthetized (0,5mg avertin/1g body weight, working solution: 20mg avertin/ml) mice. Avertin was administered via endoperitoneal injection. Fixation was performed with freshly prepared 4% PFA, ice cold, using a mechanical pump attached to the ventral part of the heart. After fixation, whole brain was placed in ice cold 4% PFA for 4 hours at 4^oC. Following, the whole brain was placed in 30% sucrose solution in PBS 1X at 4^oC on a shacking platform, until brain is precipitated. This step usually requires 2-3 days. Next, brains were embedded to OCT cryoprotectant chemical and subjected to cryotome, in order to obtain coronal slices of 0,20 μm thickness. Corresponding slices were subsequently immunostained, following the previously described method (see Immunostaining section). The following primary antibodies were used: bIII-tubulin (1:5000, mouse monoclonal, Santa Cruz, SC-80005), LC3 (Sigma-Aldrich), RAB18 (Proteintech), MAP2 (Synaptic Systems). The used secondary antibodies were: anti-rabbit Alexa 488, anti-mouse Alexa 594, and anti-guinea pig Alexa 647 (Abcam), whereas both HOECHST and BODIPY493/503 dyes were used as well. Confocal images of fluorescently labeled proteins were obtained using the Leica TSC SP8 inverted confocal microscope.

Immunoprecipitation

Immunoprecipitations were performed as previously described[92], with small modifications. Briefly, indicated lysates were pre-cleared for 1 hour by incubation with 20μl of protein G agarose beads on a rotator overnight (O/N) at 4^{o}C. Then, pre-cleared lysates were incubated with 30μl of freash beads conjugated with an antibody against RAB18 (Proteintech) or PLIN2 (Proteintech), O/N on a rotator at 4^{o}C. Ensuing, beads were washed with ice cold PBS 1X and spinned down, in order for their supernatant to be analyzed by Western blot. As a positive control of the method, no antibody conjugation beads and IgG (flowthrough) were immunobloted in parallel.

Western blotting

Western blot analysis was performed as previously reported[92]. Briefly, tissues were collected in ice cold PBS 1X and lysed by sonication in RIPA buffer (50 mM Tris-HCl pH=7.2, 150mM NaCl, 1mM EDTA, 1% Triton 100-X, 0.1% Na-deoxycholate, 10% SDS), supplemented with protease inhibitors (PIs) (Roche). Tissues were incubated O/N at 4^{o}C, whereas the next day are centrifuged for precipitating any debris, and the supernatant is supplemented with Laemli buffer, boiled for 5min at 95^{o}C and loaded for analyses. Cell lysates are treated the same way, except for the sonication, that it is not required. Also, the O/N incubation in RIPA/PIs buffer is limited to 1 hour at 4^{o}C. Samples were separated on a 10%, 15% or 18% polyacrylamide gel and transferred to a nitrocellulose membrane (Millipore, 0.2μm diameter). After blocking for 1 hour at RT in 5% skim milk, membranes were incubated in the primary antibodies overnight at 4^{o}C. The following primary antibodies were utilized: LC3 (Santa Cruz, Sigma-Aldrich), p62 (PROGEN), RAB18

(Proteintech), PLIN2 (Proteintech), Synj1 (1:1000, rabbit polyclonal, Synaptic Systems, #145003), Syn1 (1:1000, rabbit polyclonal, NovusBio), Syn2 (1:1000, mouse monoclonal, Synaptic Systems, #106211), SAP102 (DLG3) (1:1000, rabbit polyclonal, Synaptic Systems, #124213), FIP200 (1:1000, rabbit monoclonal, Cell Signaling), CFL1 (1:10000, mouse monoclonal, Proteintech, #66057-1-1g), GABARAPL1 (1:1000, rabbit monoclonal, Cell Signaling, 26632), Pvalb (1:1000, goat, Swant, PVG-214), Calb2 (1:1000, rabbit polyclonal, Swant, 7699/4), Shank1 (1:1000, rabbit polyclonal, Synaptic Systems, 162002), TATA binding protein (1:1000, mouse monoclonal, Abcam, ab61411), GRP78 Bip (1:1000, rabbit polyclonal, Abcam, ab21685), Gapdh (1:500, mouse monoclonal, Santa Cruz, sc-47724), actin (1:5000, mouse monoclonal, Santa Cruz, SC-58673), bIII-tubulin (Santa Cruz). After three 10 min washes in PBS/T (PBS 1X, 0.1% Tween-20), membranes were incubated for 1 hour at RT in corresponding secondary horseradish peroxidase-conjugated antibodies (1:10000, Abcam or Sigma, in 2% skim milk in PBS/T). After 3 subsequent 10 min washes with PBS/T, membranes were developed by chemiluminescence (Supersignal chemiluminescent substrate, pico and fempto, Thermo Fisher Scientific) according to the manufacturer's instructions. For GABARAPL1 antibody, the specific manufacturer's instructions were followed for the blocking, incubation and washes of membrane blots.

Ex vivo autophagy assay

Male animals of indicative postnatal day and of C57BL/6 genetic background were sacrificed and their whole brains (apart from cerebellum and olfactory bulbs) were submitted to vibratome, in order to obtain slices of 100μm thickness. For the Baf A1 treatment, only one male animal was used (P25), and the one sides of the slices were maintained in oxygenated cerebrospinal fluid

alone, while the other sides were supplemented with 10nM of Baf A1 (Sigma-Aldrich) for 3 hours. Explants were processed for isolation of lysates, as described (see section Western blotting). This sample was used for the Figure S6 immunoprecipitation experiment. [This ex vivo experiment was performed by Vassiliki Nikoletopoulou, PhD]. For the NMDA and DHPG treatments, slices from 15 male animals (P25) were used, each 5 for 3 different cases (control, NMDA and DHPG treatments), and subsequently treated with the respective agonists (50μM, 10min), in oxygenated artificial cerebrospinal fluid. Next, the slices were submitted to autophagosomal isolation, which is described below. [This ex vivo experiment was performed by Emmanouela Kallergi, PhD and Akrivi-Dimitra Daskalaki, MSc]. The autophagosomes that derived from this treatment were used as samples for Figure 7A.

Isolation of purified autophagosomes and nuclei

The isolation of pure autophagosomes was performed as previously described, from our laboratory established method[92]. Briefly, at least 10 male animals of indicative postnatal day and of C57BL/6 genetic background were sacrificed and their forebrains were dissected on ice and collected in 25ml of 10% (w/v) sucrose, 10mM HEPES and 1mM EDTA. After homogenization, using Dounce glass homogenizer, the homogenate was diluted with half volume of homogenization buffer (HB) (250mM sucrose, 10mM HEPES, 1mM EDTA pH 7.3) containing 1.5mM glycyl-L-phenylalanine 2-naphthylamide (GPN) in order to achieve a final GPN concentration of 0.5mM. The material was incubated at 37^{o}C for 10min, in order to achieve the osmotically disruption of lysosomes; then the material is cooled at 4^{o}C. After two centrifugations, 2000 g for 2min, the nuclei are pelleted and the supernatant is collected. The following steps include discontinuous Nycodenz, Percoll and Optiprep gradients for finally

obtaining pure autophagosomes, using Sorvall hypercentrifuge (AH-629, 36-38ml tubes) . The intermediate isolated fractions are kept for quality analysis. For analyzing the supernatant and the membrane pellet of the AV, carbonate extraction was performed, as previously described[92]. 100 μg of AVs were incubated with freshly made 0.1M sodium carbonate for 30min on ice. Next, the material was centrifuged at 20psi for 30min in an airfuge centrifug. The pellet was resuspended in Laemmle buffer and the proteins of the supernatant were precipitated, using 10% TCA. After 20 min incubation on ice, the material was centrifuged at 13,000rpm for 20 min at 4^{o}C and the pellet was washed with 100% acetone. Pellets were then left to air-dry and resuspended in Laemmle buffer. Both pellets and TCA-precipitated supernatants were in the end boiled at 95^{o}C for 5min and loaded for western blot analysis. Nuclei isolation is an established method of our laboratory, developed by Akrivi-Dimitra Daskalaki, MSc. Briefly, forebrain tissues from indicated male animals of C57BL/6 genetic background were dissected and collected in ice cold PBS 1X. Tissues are minced and transferred to PBS 1X/PIs solution (stock 25X PIs to final working solution of 1X, Roche) and centrifuged 3 times; the subsequent pellet was resuspended in cell lysis buffer (0.25M sucrose, 50mM Tris-HCl pH=8, 5mM $MgCl_2$, 2mM KCl, 0.1% NP-40, 1mM DTT (dithiothreitol), 1X PIs) and homogenized with Dounce glass homogenizator (about 20 strokes). Next, the homogenate was filtered through nylon mesh, 75 μm, with the final added cell lysis buffer amount not to exceed 10ml. The rinsed homogenate was incubated on ice for 20 min and after a centrifuge of 3 min at 1100g at 4^{o}C, the pellet is resuspended in 5 ml nuclei purification buffer (0.25M sucrose, 50mM Tris-HCl pH=8, 5mM MgCl2, 25mM KCl, 1X PIs) and gently homogenized in a Dounce glass homogenator (about 5 strokes). Following, discontinuous gradients of Percoll are used in a Sorvall hypercentrifuge (AH-629, 36ml tubes, 1hour, 16000 g, 4^{o}C). Lastly, the nuclei are pelleted by 3 concomitant centrifugations (1100g,

5min, 4^{o}C), nuclei pellets are resuspended in HB buffer. The intermediate fractions from the isolation are kept for quality control. [The nuclei isolation was performed by Akrivi-Dimitra Daskalaki]. These nuclei samples were used as samples for Figure 7E.

QUANTIFICATION AND STATISTICAL ANALYSIS

All experiments reported were performed at least one time. When the graph contains error bars, the corresponding experiments were performed 2-3 times. All samples represent biological replicates and N values are indicated in figure legends. When applicable, statistical analyses were performed with the GraphPad Prism 6 software, and the data are presented as mean ± SD. For statistical significance of the differences between the means of two groups, we used unpaired Student's t tests. For the quantification of both confocal images and blots, ImageJ software was used and in figure legends the measurement is mentioned (either diffuse signal, or puncta).

Results

RAB18 and PLIN2 LD markers are associated to autophagy and may represent different LD populations in primary neurons

We utilized RAB18 and PLIN2 antibodies as exclusive LD markers. PLIN2 is well documented as a specific LD marker, since it is located to the surface of LDs in numerous cell types[76]. As far as RAB18 is concerned, it has been previously described as an LD resident protein in non-neuronal cell models[57,63], and it is highly recommended as an exclusive LD resident protein[64]. In addition, BODIPY493/503 stains neutral lipids, and is widely used as a lipid droplet (LD) marker in a variety of cell types[93,94], including neuronal cells[88]. To clarify that RAB18 and PLIN2 associate with the presence of LDs in neurons, cortical mature and immature neurons were immunostained against both antibodies, respectively, as they also stained with BODIPY 493/503. In basal conditions, RAB18 and PLIN2 colocalize with BODIPY 493/503 (yellow puncta), providing evidence that RAB18 may be located on LDs surface in primary neurons (Figure 1A).

To test the hypothesis that RAB18 and PLIN2 are connected to macroautophagy, a direct link was searched. According to the in silico identification of functional LC3 Interacting Region Motifs (iLIR) database[95], both RAB18 and PLIN2 span one or two LIR motives respectively (Figure 1B). The LIR motif of RAB18 protein was further indicated as functional by immunoprecipitation with RAB18 in cell (*div21*) lysates, treated with BafA1, and proved that RAB18 co-immunoprecipitate with LC3 and p62 (Figure 1C). However, PLIN2 LIR motives were not verified as functional, since PLIN2 failed to co-immunoprecipitate with LC3 (Figure 1D). RAB18 was further validated as an interactor of LC3, by the positive indication that

RAB18-conjugation in beads immunoprecipitate RAB18 as well (Figure 1E). In a next step, the protein expression of both RAB18 and PLIN2 in a variety of day *in vitro* cell lysates was investigated, with the purpose of revealing any potential expression pattern in immature versus mature neurons. To our surprise, PLIN2 protein immunoblotting gives two specific bands in two different molecular weights, around 48kDa and below 63kDa. A likely explanation is that PLIN2 may have post-translational modifications. Hereafter, the 48kDa isoform is going to be mentioned as short isoform-PLIN2 (s-PLIN2), while the other as long isoform PLIN2 (l-PLIN2). The protein levels of RAB18 and s-PLIN2 decline gradually as the day *in vitro* of the culture increases (Figure 1F). Interestingly, l-PLIN2 is expressed in higher amount in *div21* compared to *div6*. Compared to the BODIPY staining levels in different day *in vitro* neuronal cultures (Figures 1A), it is proposed that mature neuronal cell cultures are more suitable as an experimental condition for exploring the role of LDs in neurons. To specify that these two proteins colocalize as LD markers, neurons were immunostained against RAB18 and PLIN2 simultaneously. Remarkably, there was little if not any colocalization between RAB18 and PLIN2 (Figure 1G), promoting the idea of different LD populations with distinct roles in primary neuronal cells.

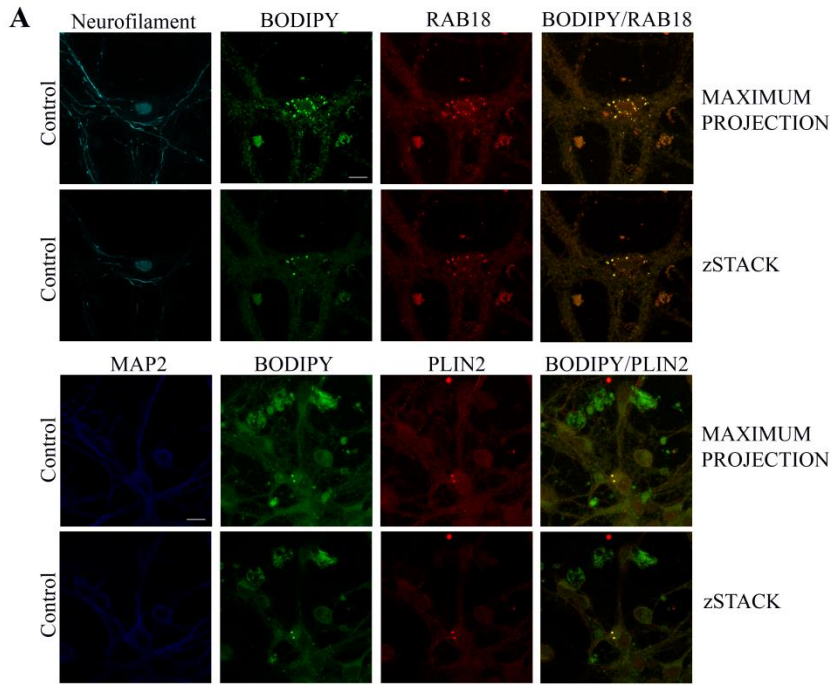
A
Neurofilament
BODIPY
RAB18
BODIPY/RAB18
Control
MAXIMUM PROJECTION
zSTACK
MAP2
PLIN2
BODIPY/PLIN2

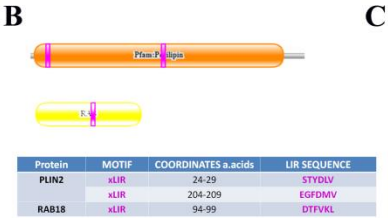
B
Protein | MOTIF | COORDINATES a.acids | LIR SEQUENCE
PLIN2 | xLIR | 24-29 | STYDLV
xLIR | 204-209 | EGFDMV
RAB18 | xLIR | 94-99 | DTFVKL

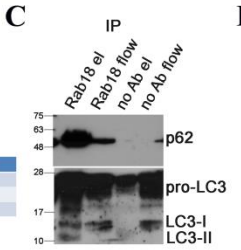
C
IP
Rab18 el
Rab18 flow
no Ab el
no Ab flow
p62
pro-LC3
LC3-I
LC3-II

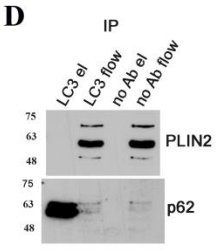
D
IP
LC3 el
LC3 flow
no Ab el
no Ab flow
PLIN2
p62

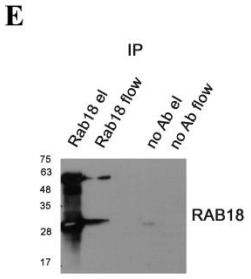
E
IP
Rab18 el
Rab18 flow
no Ab el
no Ab flow
RAB18

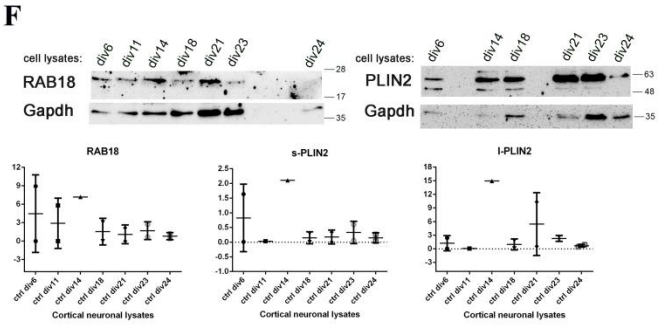
F
cell lysates:
div6
div11
div14
div18
div21
div23
div24
RAB18
Gapdh
PLIN2
RAB18
s-PLIN2
l-PLIN2
Cortical neuronal lysates

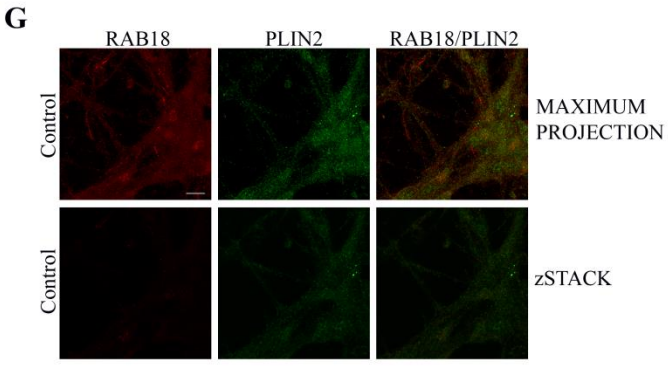
G
RAB18
PLIN2
RAB18/PLIN2
Control
MAXIMUM PROJECTION
zSTACK

Figure 1 RAB18 and PLIN2 associate with autophagy, potentially representing distinct LD populations
(A) Cortical in vitro cultured neurons, div23, are immunostained with RAB18 and Neurofilament antibodies, while concomitantly dyed with BODIPY 493/503. Similarly, cortical in vitro cultured neurons, div6, are immunostained with PLIN2 and Neurofilament antibodies, while concomitantly dyed with BODIPY 493/503. In both cases, colocalization of RAB18 and PLIN2 is observed with BODIPY 493/503 (yellow puncta).
(B) LIR motives of PLIN2 and RAB18. Image was adapted from iLIR database (http://repeat.biol.ucy.ac.cy/iLIR/).
(C) Immunoprecipitation of RAB18-conjugated beads and subsequent immunoblotting for detecting p62 and LC3 antibodies. The LC3 antibody recognizes three bands: an upper band of approximately 23 kD corresponding to pro-LC3, a middle band of 18 kD corresponding to LC3-I, and a fainter lower band of 14 kD corresponding to the lipidated LC3-II, the species that is incorporated in autophagosomes, while p62 represents a band of ~62kD. Cell lysates *div21* treated with Baf A1 was used as sample input.
(D) Immunoprecipitation of LC3 -conjugated beads and subsequent immunoblotting for detecting p62 and PLIN2 antibodies. The PLIN2 antibody recognizes two bands, one below 63 kD , while the other ~48kD. Cell lysates *div21* treated with Baf A1 was used as sample input.
(E) Immunoprecipitation of RAB18-conjugated beads and subsequent immunoblotting for detecting RAB18 antibody. The RAB18 antibody recognizes a band at 23kD, a faint band below 28kD in this figure. Cell lysates *div21* treated with Baf A1 was used as sample input.
(F) Cortical neurons of several days *in vitro* were immunoblotted for RAB18 and PLIN2 and normalized to Gapdh quantity (37kD). Graphs represent the quantification. In cases error bars exist, two independent experiments were performed (N=2). If else, one experiment is performed.
(G) Cortical in vitro cultured neurons, div6, are immunostained with RAB18 and PLIN2 antibodies. Colocalization between RAB18 and PLIN2 is not observed.
When applied, statistical analysis was implemented by using unpaired Student's t test. From the statistical test, no statistical significance is reported. Graphs are representing by mean ± SD. Scale bar=10μm. Maximum projection of z-Stacks or z-Stacks representation is indicated in each image panel.

Lipophagic flux process in cultured primary neurons under basal conditions

In cultured primary neurons autophagic flux can be measured by treating the cells with Bafilomycin A1 (Baf A1), a selective inhibitor of autophagosome-lysosome fusion[96]. To determine whether lipophagic flux is an ongoing process in neurons under basal conditions, control or BafA1-treated neurons (day *in vitro* 6 or 23 -*div6* or *div23*) were stained with the lipophilic BODIPY493/503 dye. Consequently, neurons were immunostained against autophagic markers p62 and LC3, for indicating autophagic cargo and autophagosomes respectively (Figures 2A-D). Though not significant, BafA1 led to an increase of BODIPY493/503, suggesting that there is a trend of lipid droplet accumulation in neurons when the autophagic degradation pathway is attenuated. Lipophagic flux was also tested with LD marker RAB18. For this purpose, immature neurons were treated with Baf A1 and subsequently immunostained against RAB18 (Figure 2E). Similarly, mature neurons were immunostained against RAB18 and LC3

antibodies, after Baf A1 treatment (Figure 2F and 2G). In both cases, RAB18 shows a slight elevated tendency, supporting that lipophagic flux is a constant process in neurons, under baseline conditions.

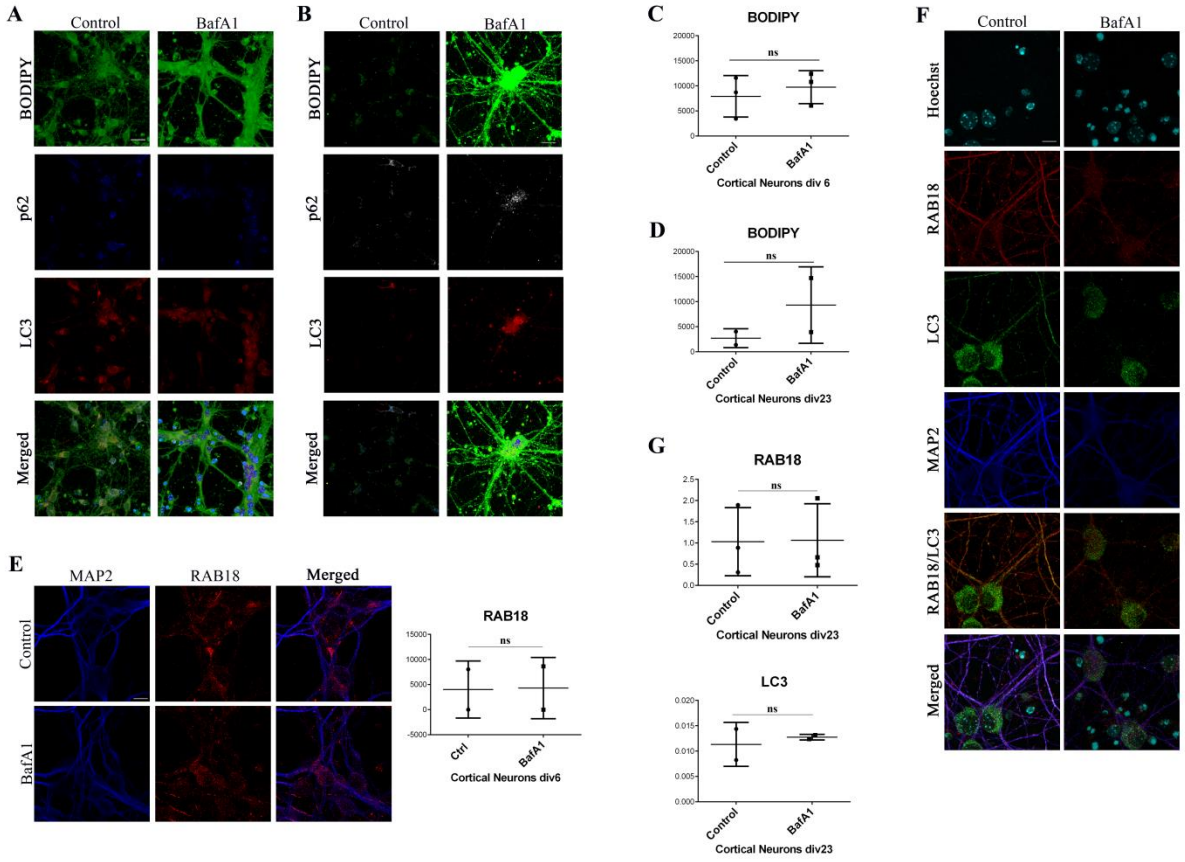

Figure 2 Lipophagic flux in primary neurons under basal conditions

(A) Cortical in vitro cultured neurons, *div6*, are untreated or treated for 6 Hrs with Baf A1 (10nM). They immunostained against LC3 and p62 antibodies, while concomitantly dyed with BODIPY493/503 and Hoechst. Merged image represent BODIPY/p62/LC3/Hoechst.
(B) Cortical in vitro cultured neurons, *div23*, are untreated or treated for 6 Hrs with Baf A1 (10nM). They immunostained against LC3 and p62 antibodies, while concomitantly dyed with BODIPY 493/503 and Hoechst. Merged image represent BODIPY/p62/LC3/Hoechst.
(C) Graph representing the quantification of Fig 2A images. Normalization was not performed. Three independent experiments were performed (N=3).
(D) Graph representing the quantification of Fig 2B images. Normalization was not performed. Two independent experiments were performed (N=2).
(E) Cortical in vitro cultured neurons, *div6*, treated with Baf A1 (10nM) for 6 Hrs, are immunostained against RAB18 and MAP2 antibodies. Graph represents the quantification, where RAB18 and LC3 were normalized to MAP2 signal, for diffused and punctuated signal respectively. Two independent experiments were performed (N=2). Merged image represent RAB18/MAP2.
(F) Cortical in vitro cultured neurons, *div23*, are treated with Baf A1 (10nM) for 6 Hrs, and subsequently immunostained against RAB18, LC3 and MAP2 antibodies, while concomitantly dyed with Hoechst. Merged image represent RAB18/MAP2/LC3/Hoechst.
(G) Graphs represent the quantification of Fig 2F images, where RAB18 and LC3 were normalized to MAP2 signal, for diffused and punctuated signal respectively. Two to three independent experiments were performed (N=2 for LC3, N=3 for RAB18).

When applied, statistical analysis was implemented by using unpaired Student's t test. From the statistical test, no statistical significance is reported. Graphs are representing by mean ± SD. Scale bar=10μm. Maximum projection of z-Stacks is represented in each image panel.

Accordingly, PLIN2 levels were also considerably increased under Baf A1 supply (Figure 3A), further support the physiological role of lipophagy. However, even under BafA1 treatment conditions, PLIN2 shows no colocalization with p62 (Figure 3A, z-STACKS). Hence, a different adaptor, Alfy, was considered to be colocalized with PLIN2 in immature neurons. Still, PLIN2 fails to colocalize with Alfy, under basal and Baf A1 conditions (Figure 3B, z-STACKS), although its levels appear to increase in line with Alfy pattern. Lipophagic flux was also assessed in cell lysates from immature (*div6*) and mature (*div21*) neurons, after Baf A1 treatment. RAB18 protein levels in *div6* neurons demonstrate a significant rise (Figure 3C), whereas Baf A1 treatment of mature neurons, lead to a considerable surge of l-PLIN2 levels and a slight increase of s-PLIN2 (Figure 3D).

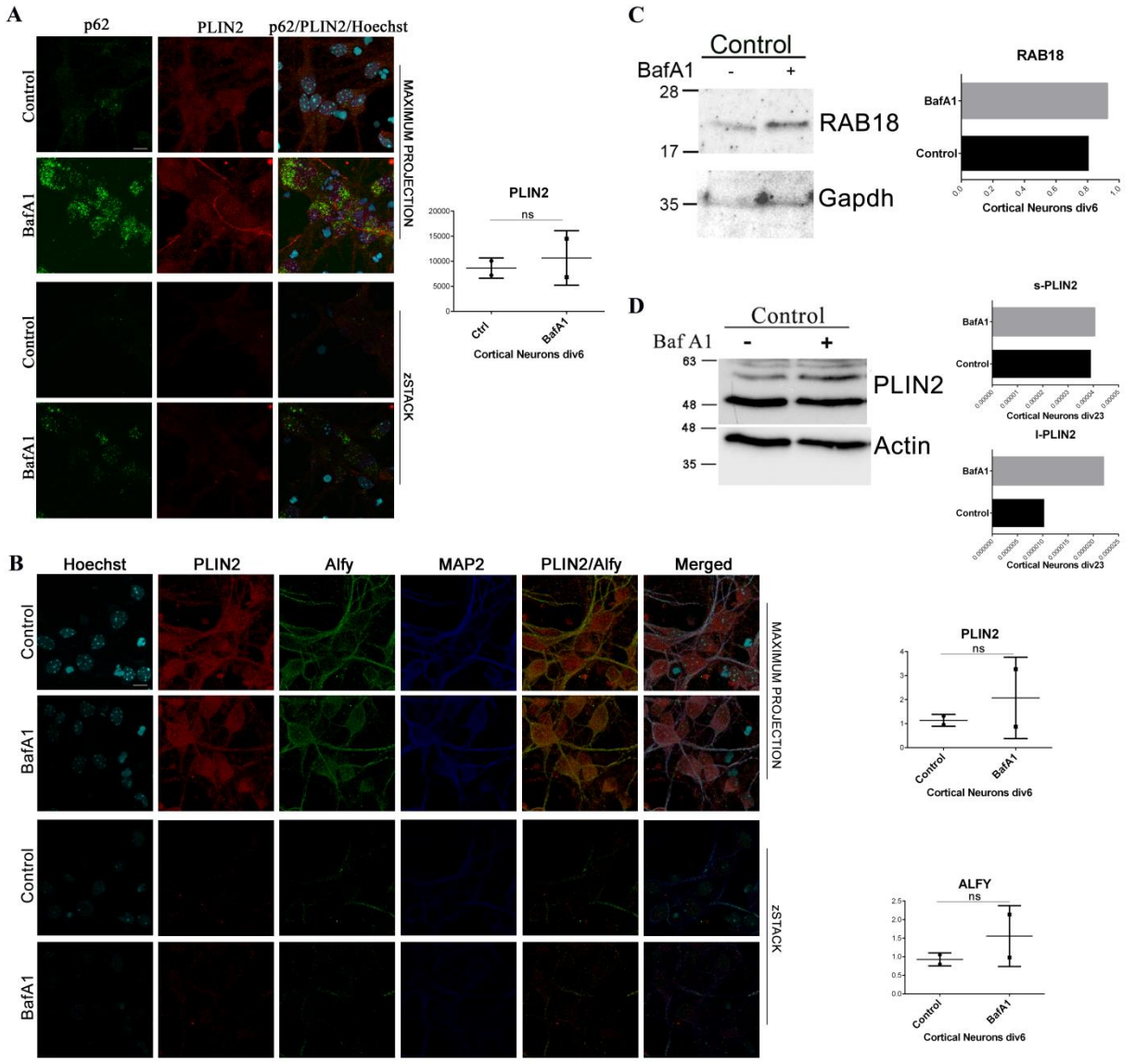

Figure 3 Lipid droplets appear to sequestered via autophagy in primary neurons under basal conditions

(A) Cortical in vitro cultured neurons, div6, treated with Baf A1 (10nM) for 6 Hrs, are immunostained with PLIN2 and p62 antibodies. p62 protein levels at the BafA1 treatment case were used as a positive treatment control. Graph represents the quantification. Two independent experiments were performed (N=2).

(B) Cortical cultured neurons, div6, were immunostained against PLIN2, Alfy and MAP2 antibodies, while dyed with the nuclear marker Hoechst. There was not observed any colocalization of Alfy and PLIN2. Graphs represent the quantification, where PLIN2 and Alfy were normalized to MAP2 signal, for punctuated signal.

(C) Cortical neuronal lysates, *div6*, untreated or treated with Baf A1 (10nM) for 6 Hrs, are immunobloted against RAB18 (normalized to Gapdh). Graph represents the quantification. One experiment was performed.

(D) Cortical neuronal lysates, *div21*, untreated or treated with Baf A1 (10nM) for 6 Hrs, are immunobloted against PLIN2 (normalized to Gapdh). Graphs represent the quantification. One experiment was performed.

Statistical analysis was implemented by using unpaired Student's t test. From the statistical test, no statistical significance is reported. Graphs are representing by mean ± SD. Scale bar=10μm. Maximum projection of z-Stacks or z-Stacks is indicated in each image panel.

Fasting conditions regulate lipophagic flux in primary neurons

Nutrient deprivation is a well-established autophagic stimulus in neuronal cells[97]. It is known that, when starvation is induced *in vitro* neuronal cell cultures, autophagy is enhanced[96]. Therefore, we set out to investigate if lipophagic flux is affected under starved settings. Fasted conditions (24 Hrs) were tested in mature primary neurons, which were immunolabeled against RAB18, p62 and Neurofilament, as they were concomitantly stained with BODIPY 493/503 (Figure 4A). It is observed an augmented colocalization between RAB18, BODIPY 493/503 and p62 under stressed conditions (yellow and magenta puncta respectively), highlighting that stress may induce the LD accumulation in primary neurons. In mature neurons, no colocalization of RAB18 and p62 in basal conditions is detected (Figure S1). Interestingly, under fasting conditions, both BODIPY 493/503 and RAB18 intensities are extensively elevated, though p62 levels are not significantly diminished, underlining a possible buffering role of LDs in alleviating cellular lipotoxicity, provoked by prolonged autophagic activation, as previously suggested[98]. Since 24Hrs of fasting may lead to neuronal apoptosis, smaller starvation periods were tested (Figure 4B). Consistent with the 24 Hrs fasting results, RAB18 and LC3 are colocalized after 6 Hrs starvation, while this colocalization is missing after only 45 min fasting. RAB18 protein levels are augmented under 45min and 6 Hrs starvations, as also LC3 levels, supporting that RAB18 may be regulated positively, when autophagy is enhanced. Another stress factor is the supplementation of oleic acid in neuronal cell cultures[88]. In fact, oleic acid treatment promotes the punctuation and colocalization of BODIPY, RAB18 and p62 (Figure S2A). PLIN2 demonstrates the same response, as its signal appears to be more punctuated and the colocalization (yellow puncta) with LC3 is prominent (Figure S2B). Nevertheless, even colocalization of RAB18 and PLIN2 is observed under oleic acid administration in mature

neurons (Figure S2C). All together, these effects provide a solid assumption that autophagy influences RAB18 and PLIN2 proteins in primary neurons, supporting lipophagy as a physiological mechanism, while stress conditions alternate their expression and maybe their function.

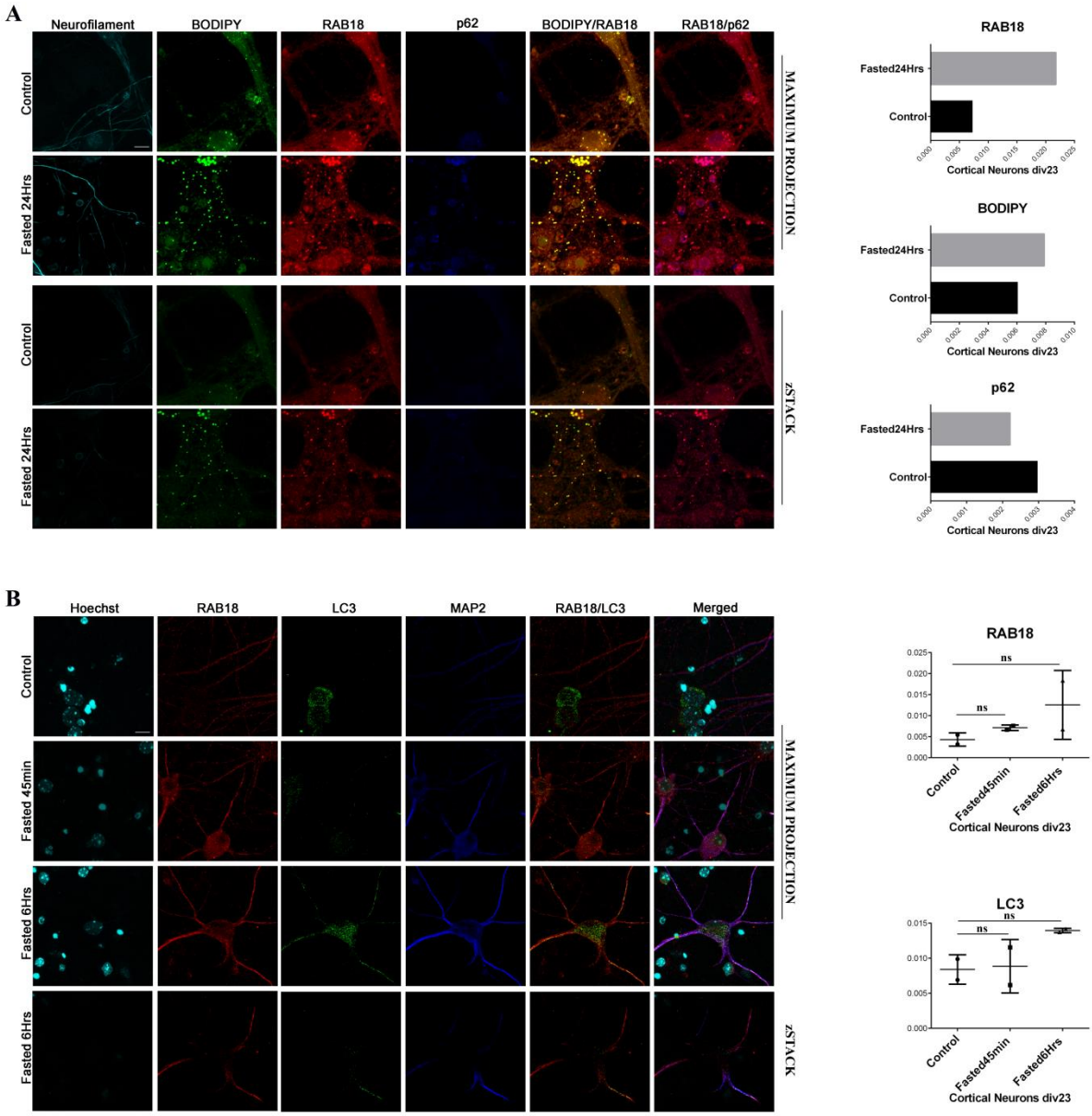

Figure 4 Prolonged fasting conditions increase RAB18 protein levels and colocalization with LC3 or p62

(A) Cortical in vitro cultured neurons, *div23*, are fasted for 24 Hrs. Then, they are stained with RAB18, p62 and Neurofilament antibodies, while concomitantly dyed with BODIPY 493/503. Colocalization of RAB18 with BODIPY493/503 and p62 is observed. Graphs represent the quantification, where RAB18 , BODIPY493/503 and p62 were normalized to Neurofilament signal, for punctuated signal all three.

(B) Cortical in vitro cultured neurons, *div23*, are fasted for 45 min or 6 Hrs. Then, they are stained with RAB18, LC3 and MAP2 antibodies. Colocalization of RAB18 and LC3 is observed only under 6 Hrs starvation. Graphs represent the quantification, where RAB18 and LC3 were normalized to MAP2 signal, for punctuated signal all three.

When applied, statistical analysis was implemented by using unpaired Student's t test. From the statistical test, no statistical significance is reported. Graphs are representing by mean ± SD. In cases error bars exist, two independent experiments were performed (N=2). If else, one experiment is performed. Scale bar=10μm. Maximum projection of z-Stacks or z-Stacks representation in each image panel.

On top of that, we sought to explore if a smaller fasting time periods alters lipophagic flux pattern. Interestingly, when neurons are fasted for 45 min (minutes) or 6 Hrs, BODIPY 493/503 intensity is sharply dropped only after 45 min treatment (Figure 5A), pointing out that LDs may follow the autophagic degradation pathway for their sequestration, for this starvation period. Conversely, after 6 hours starvation, BODIPY 493/503 was largely enhanced, in line with previous evidence that supported LD accumulation in prolonged fasted periods[98]. Additionaly to cultured neuronal cells, cortical tissue slices from wild-type male animals, 2 months old (postnatal day 60 – P60), fed and fasted for 24 Hrs, were stained with BODIPY 493/503 dye and co-immunostained for βIII-tubulin (Tuj1) and MAP2, so as to monitor both axons and dendrites of neurons (Figures 5B). Tissue slices consist of both neurons and glial cells, compared to pure neuronal cell cultures. It has been already defined that autophagy is inhibited in the cortex of mature animals, under fasted conditions[92]. Unexpectedly, BODIPY 493/503 reveals a decreased tendency under fasted conditions in cortical tissue, suggesting that LDs degradation may depend on cell type specificity. Next, we wanted to see if this this autophagic effect corresponds to lysates from brain tissue, apart from *in vitro* cultured primary neurons and fixed tissue slides. To that end, forebrain tissue lysates from postnatal day 30 (P30) and postnatal day 86 (P86) wild-type animals, were immunobloted against RAB18 and PLIN2 antibodies (Figure 5C). In addition, forebrain tissue lysates from P86 wild-type animal were immunoblotted against RAB18 antibody (Figure 5D). It has been previously described that autophagy is induced in the forebrain of young animals under fasted conditions, whereas it is reduced in the forebrain of older animals[92]. Notably, both proteins exhibit a steep decrease under fasting (24Hrs) in the forebrain of P30 animals, suggesting that starvation may promote their degradation through autophagy. Treatment with BafA1 for 6 Hrs fails to rescue their levels even in basal state. Successively,

RAB18 is highly enhanced under starvation (24Hrs) in P86 animal forebrains, associating the autophagic machinery with the accumulation of RAB18.

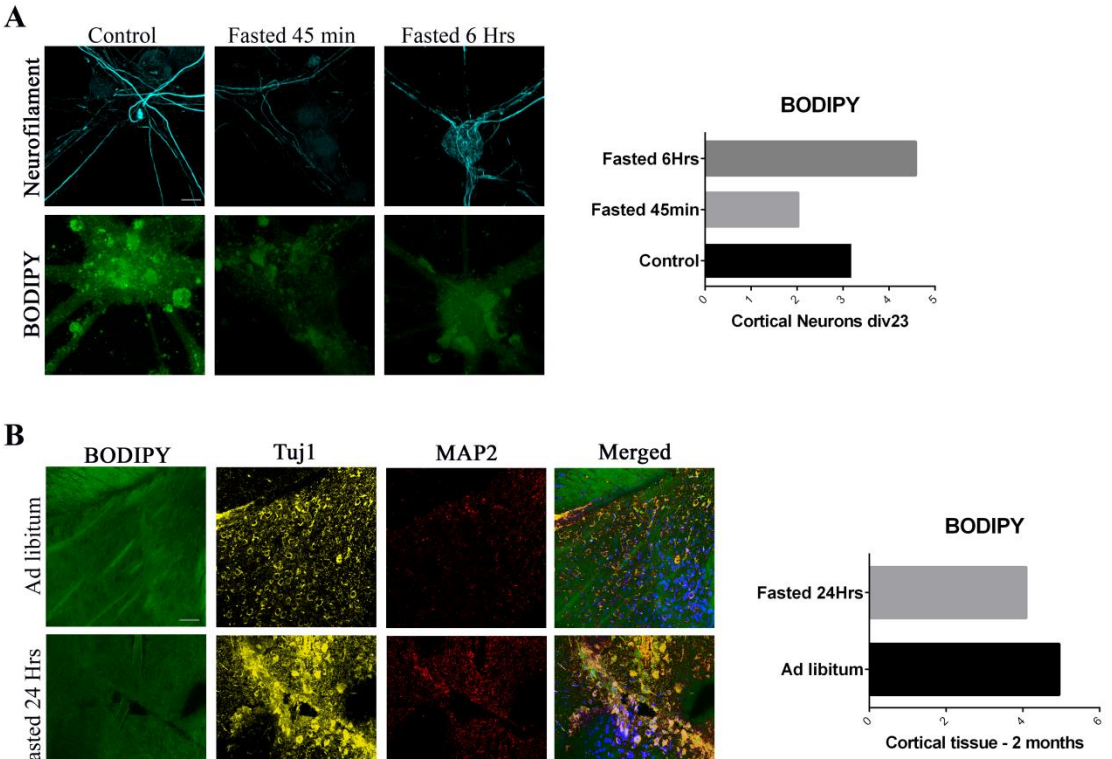
A
Control
Fasted 45 min
Fasted 6 Hrs
Neurofilament
BODIPY
BODIPY
Fasted 6Hrs
Fasted 45min
Control
0
1
2
3
4
5
Cortical Neurons div23
B
BODIPY
Tuj1
MAP2
Merged
Ad libitum
Fasted 24 Hrs
BODIPY
Fasted 24Hrs
Ad libitum
0
2
4
6
Cortical tissue - 2 months

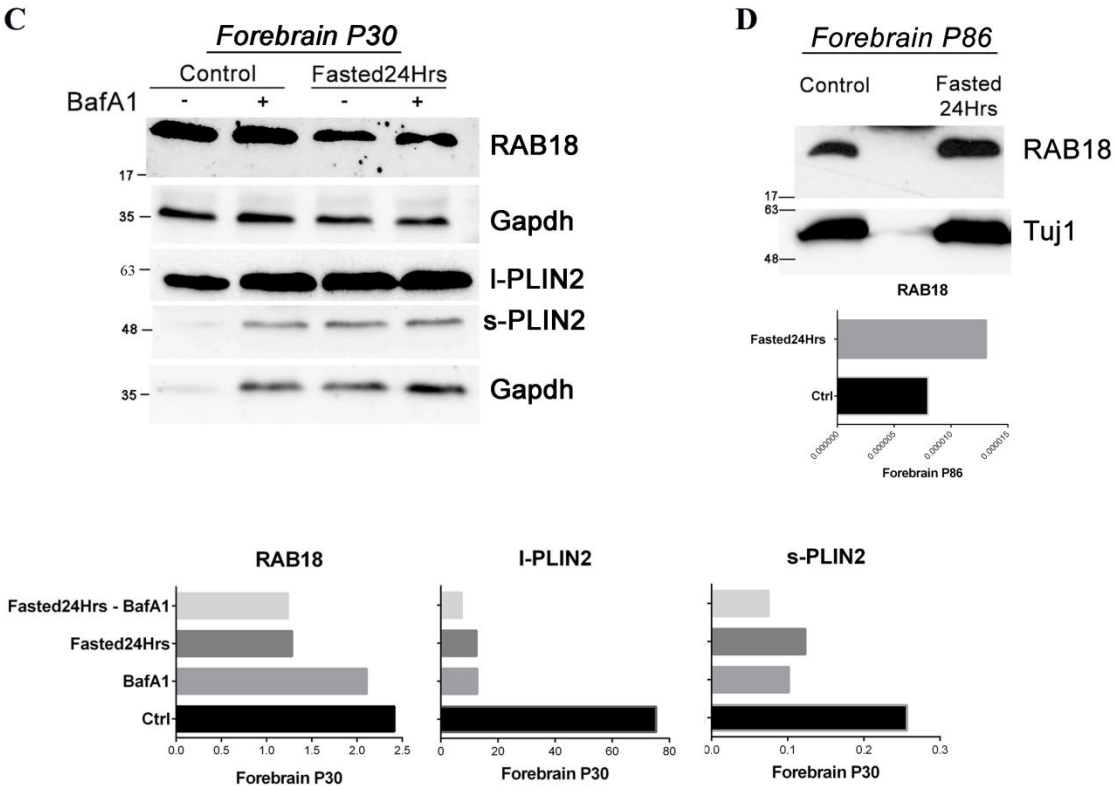
C
Forebrain P30
Control
Fasted24Hrs
BafA1
-
+
-
+
RAB18
17
Gapdh
35
l-PLIN2
63
s-PLIN2
48
Gapdh
35
D
Forebrain P86
Control
Fasted 24Hrs
RAB18
17
63
Tuj1
48
RAB18
Fasted24Hrs
Ctrl
0.000000
0.000005
0.000010
0.000015
Forebrain P86
RAB18
Fasted24Hrs - BafA1
Fasted24Hrs
BafA1
Ctrl
0.0
0.5
1.0
1.5
2.0
2.5
Forebrain P30
l-PLIN2
0
20
40
60
80
Forebrain P30
s-PLIN2
0.0
0.1
0.2
0.3
Forebrain P30

Figure 5 Mild *in vitro* starvation and *in vivo* fasting processes also support lipophagy
(A) Cortical in vitro cultured neurons, *div23*, are fasted for 45 min or for 6 Hrs, or not fasted. They concomitantly dyed with BODIPY 493/503. Graph representing the quantification of this image. Normalization was not performed. One experiment was performed.
(B) Cortical tissue of 2 months old animals, control and starved for 24 Hrs were immunostained against bIII-tubulin and MAP2, while they are also dyed with BODIPY 493/503. Graph representing the quantification of this image. Normalization was not performed. One experiment was performed.
(C) Forebrain slices of unfasted or fasted for 24 Hrs animals (P30) were treated with Baf A1 (10nM) for three hours and their lysates were immunoblotted for RAB18 and PLIN2 antibodies (normalized to Gapdh). Graphs represent the quantification. One experiment was performed.
(D) Forebrain lysates of unfasted or fasted for 24 Hrs animals (P86) were immunoblotted for RAB18 antibody (normalized to Tuj1). Graph represents the quantification. One experiment was performed.
Graphs are representing by mean ± SD. Scale bar=10μm. All images are representing maximum projection of z-STACKS.

Inhibition of autophagy in different autophagosomal biogenesis stages affects both RAB18 and PLIN2 protein levels in primary neurons

The consequences of blocked autophagy, via chemical manipulation, can be observed to immature and mature neuronal cultures. It is known that SBI-0206965 is a selective ULK1 inhibitor[99], inhibiting autophagy in the early stages of AV formation, the formation of PAS. Remarkably, RAB18 levels were significantly reduced in cortical mature neurons, after the supply of SBI (Figure 6A, middle panel and respective quantification). In line with this result, SBI treatment of mature cortical neurons causes a small, non-significant, decrease of RAB18 and PLIN2 in cell lysates (Figure 6B). An emerging role of lipids in the formation and expansion of AVs may hold a possible interpretation of this finding. Another recently identified autophagy inhibitor is brain derived neurotrophic factor (BDNF)[92]. BDNF is widely known as a modulator of hippocampal long-term potentiation (LTP)[100,101], a continuous synaptic strengthening that enhances the processes of memory and learning. It has been reported that induced autophagy mediates synaptic defects, provoked by BDNF deficits[92]. However, BDNF has been documented that positively regulates cholesterol metabolism for the development of the synapse[102]. Therefore, our findings urged us to explore the role of BDNF in lipophagic flux in neurons.

Strikingly, treatment of mature neurons with BDNF provokes a remarkable drop in RAB18 levels (Figures 6A, right panel and respective quantification and 6C). In contrast to RAB18, PLIN2 results are inconclusive; under BDNF treatment, its two isoforms are expressed in direct opposite manner, with l-PLIN2 isoform to be encanced (Figure 6C). In line with this evidence, RAB18 translational expression was measured in cortical and cerebellum tissue lysates from control (noCre;$BDNF^{f/+}$) and *BDNF* heterozygous (NestinCre;$BDNF^{f/+}$) animals (Figure 6D). Markedly, RAB18 is increased in both tissues, supporting the notion that RAB18 is a potent positive modulator of autophagy. Nevertheless, BODIPY493/503 intensity appears to be enhanced, under BDNF treatment of mature cortical neurons (Figure 6E). Thus, we can speculate that RAB18 and s-PLIN2 may mark distinct LDs types with unknown functions, independent of their sequestration via the AV-lysosomal fusion.

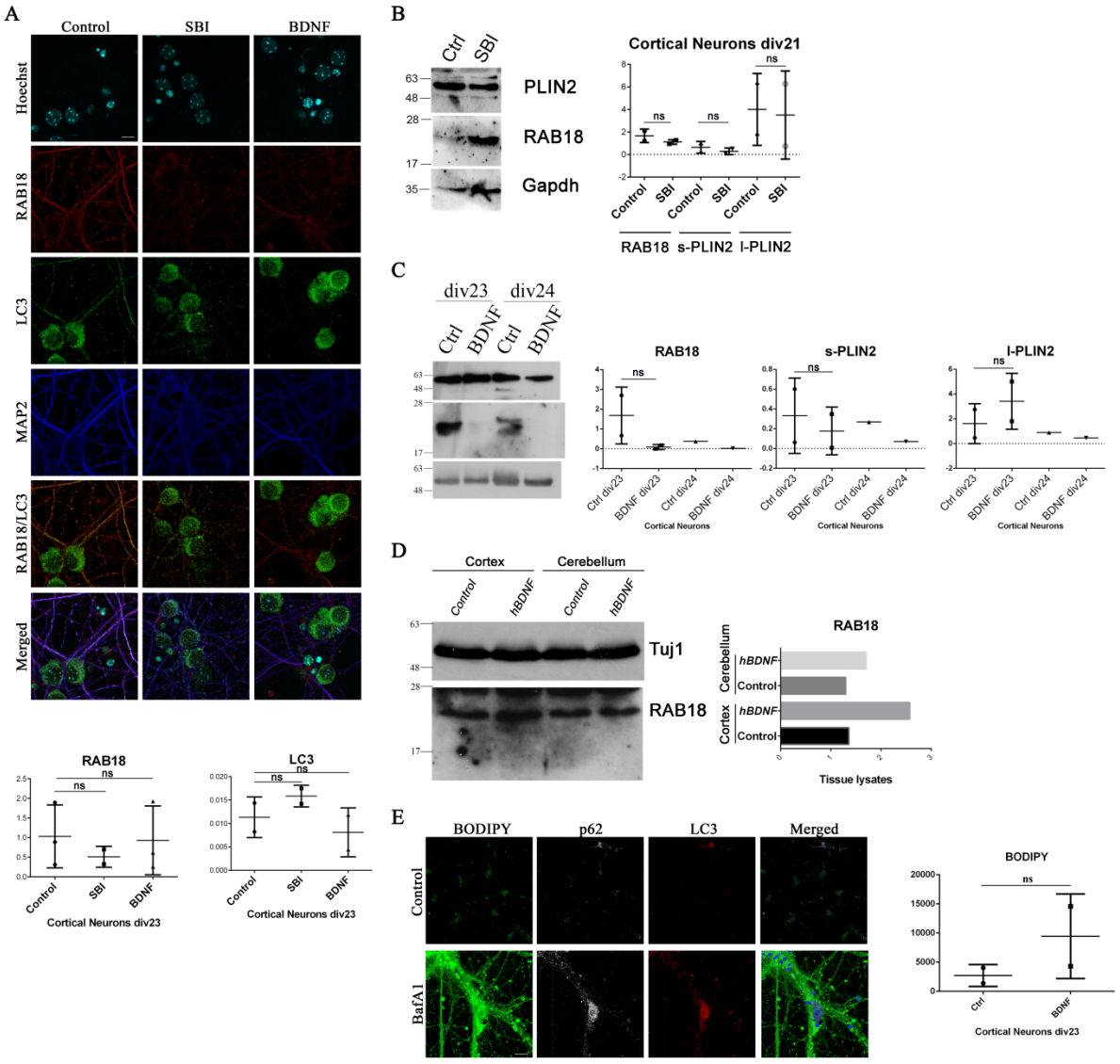

Figure 6 Inhibition of autophagy in different autophagosomal formation stages in primary neurons modulates RAB18 and PLIN2 levels

(A) Cortical in vitro cultured neurons, *div23*, were treated with SBI (500nM) for 6 Hrs or BDNF (50ng/ml) for 48 Hrs and immunostained against RAB18 and LC3 antibodies. Graphs represent the quantification, where RAB18 and LC3 were normalized to MAP2 signal, for difused and punctuated signal respectively. Two to three independent experiments were performed (N=2 for LC3 and RAB18 SBI case, N=3 for RAB18 except for SBI case).

(B) Cortical neuronal lysates, *div21*, untreated or treated with SBI (500nM) for 6 Hrs, are immunobloted against RAB18 and PLIN2 (normalized to Gapdh). Graph represents the quantification.

(C) Cortical neuronal lysates, *div23 or div24*, untreated or treated with BDNF (50ng/ml) for 48 Hrs, are immunobloted agaisnt RAB18 and PLIN2 (normalized to bIII-tubulin (Tuj1)). Graphs represent the quantification.

(D) Cortical and cerebellum lysates from control (noCre;BDNF$^{f/+}$) or *hBDNF* (NestinCre;BDNF$^{f/+}$) were immunoblotted for RAB18 antibody (normalized to Gapdh). Graphs represent the quantification.

(E) Cortical in vitro cultured neurons, *div23*, are untreated or treated for 48 Hrs with BDNF (50ng/ml). They immunostained against LC3 and p62 antibodies, while concomitantly dyed with BODIPY 493/503 and Hoechst.

When applied, statistical analysis was implemented by using unpaired Student's t test. From the statistical test, no statistical significance is reported. Graphs are representing by mean ± SD. In cases error bars exist, two to three independent experiments were performed (N=2, N=3). If else, one experiment was performed. Scale bar=10μm. All images are maximum projections of z-STACKS.

Chemical long term depression (LTD) and conditional ablation of *Atg5* gene have an impact on RAB18 and PLIN2 roles in lipophagy

Apart from LTP, synaptic plasticity is also characterized by a constant decrease of synaptic strengthening, a mechanism called long term depression (LTD)[103]. LTD elicits spine elimination and pruning, suggesting a protein degradation mechanism[104]. Two major forms of LTD require the activation of N-methyl-d-aspartate receptors (NMDARs), from L-glutamate neurotransmitter and metabotropic glutamate receptors (mGluRs) from group I mGluR agonist 3,5-dihydroxyphenylglycine (DHPG). It has been reported that the stimulation of NMDARs with NMDA agonist in a brief low dose (5 min), a form of chemical LTD, enhances autophagic responses[105]. Despite the fact that DHPG has been characterized as an activator of the mammalian target of rapamycin (mTOR) and the phosphatidylinositol-3 kinase (PI3K)[106,107], its direct connection to autophagy has not been fully addressed, especially in basal conditions. In order to address if chemical LTD affects lipophagic flux, primary neurons in *div6* where pulsed with either NMDA agonist or (S)-3,5-Dihydroxyphenylglycine (DHPG) for 5 min. NMDA and DHPG supplementation depict a slight decline in BODIPY (Figures 7A), proposing that, in induced autophagic conditions, dependent on synaptic activity, LDs are sequestered via the autophagic pathway. Strikingly, RAB18 protein levels demonstrate a steep rise under NMDA treatment in immature neurons (Figure 7B), suggesting that RAB18 may implicate to synaptic activity. Following, we sought to investigate if there are any fluctuations in RAB18 and PLIN2 protein levels in brain tissues from postnatal day 25 (P25) conditional knock-out Atg5 (*cAtg5*) and their control ($Atg5^{f/f}$) animals. The deletion of *Atg5* is shown in tissue lysates from P25 *cAtg5* and $Atg5^{f/f}$ animals (Figure S3). For this matter, tissue lysates from 3 different brain

regions (cortex, hippocampus and hypothalamus) were immunoblotted against RAB18 and PLIN2 (Figure 7C). Remarkably, there is a tendency of RAB18 decreased in levels in all tissues, suggesting an association between RAB18 and autophagosome formation. In contrast, s-PLIN2 amount appears to be elevated in all tissues, demonstrating that LDs sequestration may be impaired, when autophagy is depleted. l-PLIN2 did not show a robust result, as in cortical and hypothalamic lysates is to some extent declined, in contrast to hippocampal tissue, where it is augmented. Additional sign that RAB18 may be a positive modulator of autophagy is its substantial declined levels in striatum of *cAtg5* compared to control animals, consistent to the decreased LC3 levels (Figure 7D). Unanimously, these findings invite the speculation that autophagic activity modulates RAB18 and PLIN2 expressional patterns, while chemical LTD elucidate a potential role of RAB18 in synaptic activity.

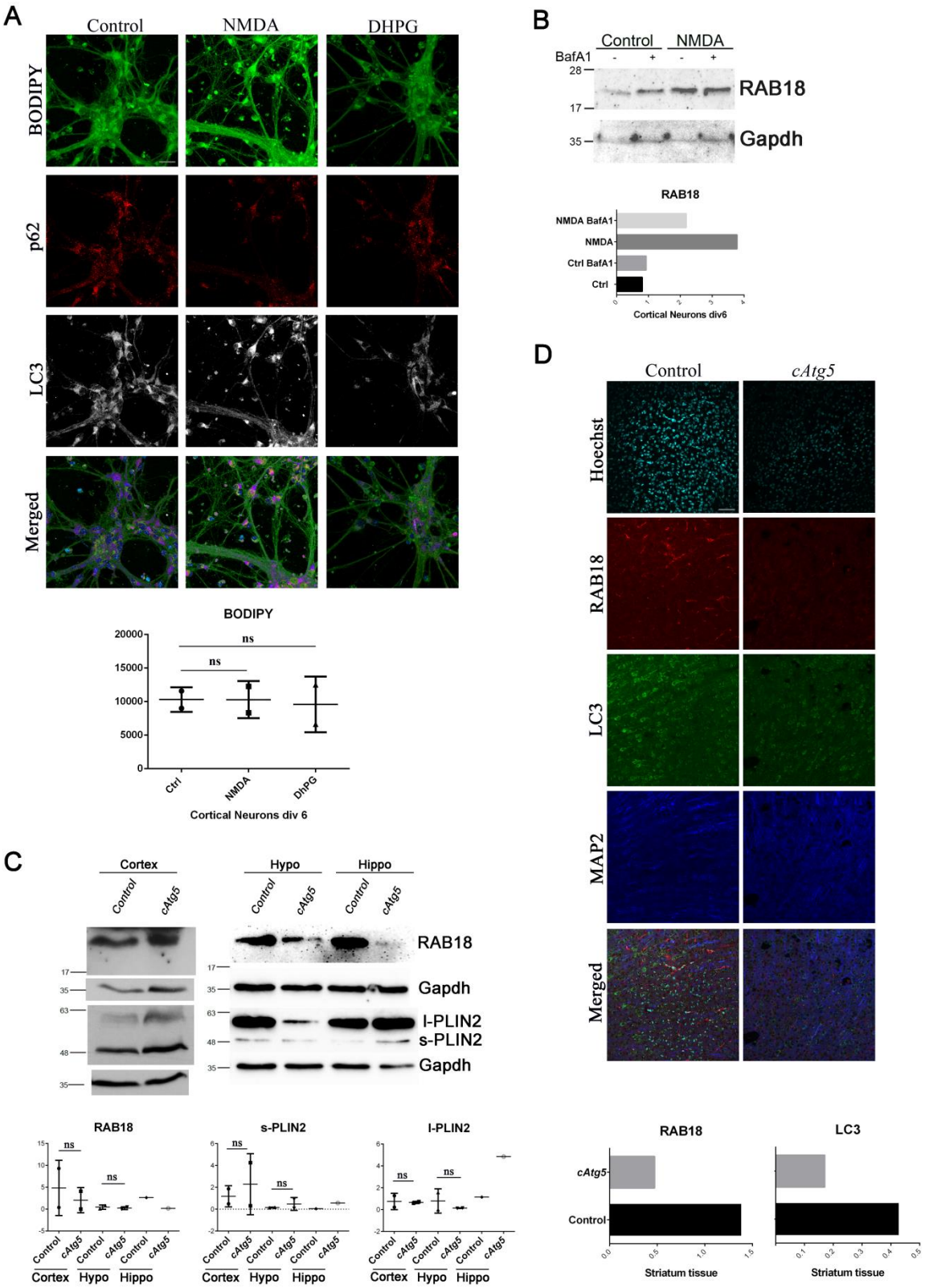
A
Control
NMDA
DHPG
BODIPY
p62
LC3
Merged
BODIPY
ns
ns
20000
15000
10000
5000
0
Ctrl
NMDA
DhPG
Cortical Neurons div 6
B
Control
NMDA
BafA1
- + - +
28
17
35
RAB18
Gapdh
RAB18
NMDA BafA1
NMDA
Ctrl BafA1
Ctrl
Cortical Neurons div6
C
Cortex
Hypo
Hippo
Control
cAtg5
RAB18
Gapdh
l-PLIN2
s-PLIN2
Gapdh
RAB18
s-PLIN2
l-PLIN2
ns
Control
cAtg5
Cortex
Hypo
Hippo
D
Control
cAtg5
Hoechst
RAB18
LC3
MAP2
Merged
RAB18
LC3
cAtg5
Control
Striatum tissue
Striatum tissue

Figure 7 Chemical LTD and ablation of *Atg5* gene implicate RAB18 and PLIN2 lipophagic roles
(A) Cortical in vitro cultured neurons, *div6*, are untreated or pulsed for 5 min with NMDA and DHPG (50μM). They immunostained against LC3 and p62 antibodies, while concomitantly dyed with BODIPY 493/503 and Hoechst. Graph representing quantification. Normalization was not performed. Two independent experiments were performed (N=2).
(B) Cortical neuronal lysates, *div6*, untreated or pulsed with pulsed for 5 min with NMDA (50μM) and subsequent treated with Baf A1 (10nM) for 6 Hrs, are immunobloted against RAB18 (normalized to Gapdh). Graph represents the quantification.
(C) Cortical, hypothalamic (hypo) and hippocampal (hipo) lysates from control (noCre;$Atg5^{f/f}$) or *cAtg5* animals (P25) were immunoblotted against RAB18 and PLIN2 antibodies (normalized to Gapdh). Graphs represent the quantification.
(D) Fixed striatum tissue from control (NestinCre;$Atg5^{+/+}$) or *cAtg5* animals (P31) were immunostained against RAB18 and LC3 antibodies. Graphs represent the quantification, where RAB18 and LC3 were normalized to MAP2 signal, for diffused signal.
When applied, statistical analysis was implemented by using unpaired Student's t test. From the statistical test, no statistical significance is reported. Graphs are representing by mean ± SD. In cases error bars exist, two independent experiments were performed (N=2). If else, one experiment is performed. Scale bar=10μm. All images are maximum projection of z-STACKS.

RAB18 is localized on the membrane of the autophagosome, while PLIN2 is present in the autophagosomal lumen

Up to now, indirect evidence is presented regarding the engulfing of LDs in the representative organelle of macroautophagy, the autophagosome (AV). To address this issue in a more straight way, pure autophagosomes (AVs) are extracted from tissue slices of P25 wild-type animals, untreated or treated with NMDA and DHPG, following a well described method[92]. Pure AVs are subsequently submitted to carbonate extraction (CE), in order to separate the inner and outer membrane from the supernatant of the AV. The purity of autophagosomes in all three cases was determined by immunoblotting for ER, cytoplasmic and nuclear markers (data not shown). Surprisingly, Western blot analysis of purified AVs, before and after CE, demonstrates that RAB18 is located to the membrane of the AV, while PLIN2 is found in the supernatant (Figure 8A). Under induced autophagic treatments (NMDA and DHPG), RAB18 and l-PLIN2 levels are elevated, while s-PLIN2 is decreased (Figure 8B). Thus, it is further supported that RAB18 and PLIN2 represent two different LD populations, which respective roles are regulated in a distinct way from the autophagic machinery. Consequently, RAB18 possible interactors were

investigated, by performing Coomassie-Blue staining in the autophagosomal membranes (Figure 8C). The immunoprecipitation of RAB18-conjugated beads with AVs either membrane pellet or supernatant input sample was successful, as the lack of bands in the no Ab elusion columns was obvious (Figure S4). Several bands in different molecular weights are detected faintly in RAB18 elusion from AVs membrane pellet, providing clues for important RAB18 protein interactors in the AV (Figure 8C). FIP200 is tested as a potential interactor of RAB18 by immunoprecipitation, considering the role of LDs in the autophagosomal biogenesis[54]. Unfortunately, RAB18 fails to directly interact with FIP200 (Figure S5), highlighting potential intermediate protein interactors between RAB18 and FIP200.

It has been described that LDs biogenesis initiate from the ER bilayer[50], where RAB18 is localized[59]. For clarifying if this belief is valid also in brain tissue, purified ER and cytoplasmic material from forebrain of P25, P60 and P180 tissues of male animals, were immunoblotted against RAB18 (Figure 8D). Importantly, RAB18 is localized almost exclusively in ER, while it is nearly absent from the cytoplasmic material. Gapdh expression is used to validate the purity of ER material, as it is unanimously expressed, except for ER. Lastly, ER is the extension of the nuclear membrane and there is a growing body of literature suggesting the existence of nuclear LDs[108]. To test this hypothesis, pure nuclei from forebrain of P25, P40 and P60 male animals were analyzed by Western blot for the presence of RAB18 protein (Figure 8E). The purity of nuclear extracts is determined by cytoplasmic and nuclear markers (Figure S6). Intriguingly, RAB18 is detected only in P25 forebrain nuclei, establishing a promising location and age-dependent role of RAB18 in the brain tissue.

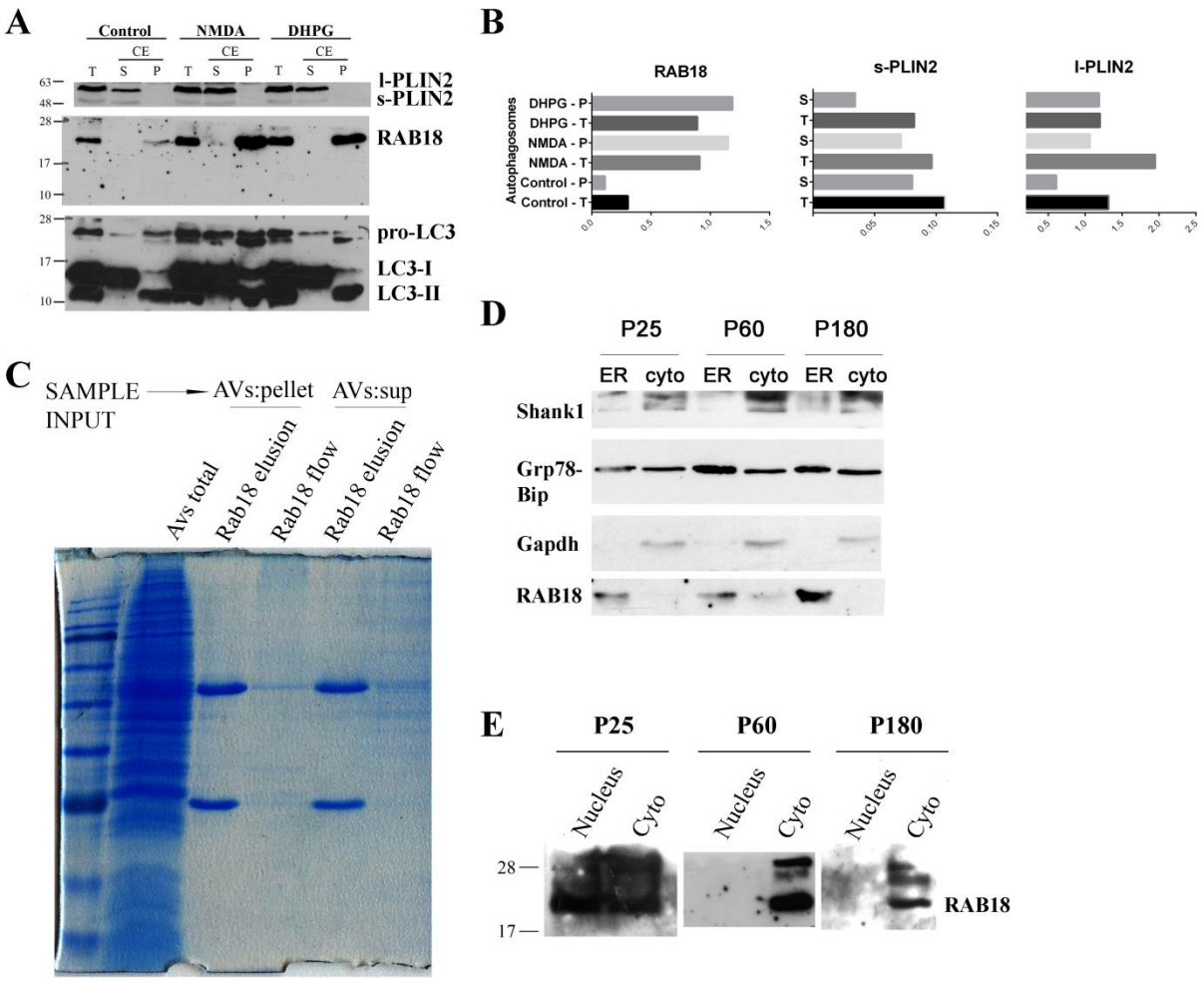

Figure 8 RAB18 and PLIN2 are located to different autophagosomal structures, whereas RAB18 localization is observed in ER and nuclei as well

(A) Total (T) autophagosomes or pellet (P) and supernatant (S) AVs fractions, purified from ex vivo treatment of forebrain slices untreated or treated with NMDA and DHPG (50μM) for 10 min, were immunoblotted against RAB18 and PLIN2 (normalized to LC3-II from pellet). In all three cases, RAB18 is observed in the (P) fraction, while PLIN2 in the (S) fraction. One experiment was performed.
(B) Graphs representing the quantification of Figure 7A. As loading control, LC3-II from (P) fraction was used for the (P) and (S) fractions, while LC3-II from (T) for the (T) fractions.
(C) Immunoprecipitation of RAB18-conjugated beads, using as sample input (P) or (S) AVs fractions and subsequent staining with Coomassie Blue dye, to identify possible RAB18 interactors.
(D) Intermediate fractions of cytoplasm (cyto) and ER from AVs isolation method, were immunoblotted against RAB18, ER marker (Grp-78 Bip) and cytoplasmic marker (Shank1) and Gapdh (positive marker of only cytoplasmic material). RAB18 is localized exclusively to the ER fraction.
(E) Forebrains from male animals of indicative postnatal days were submitted to nuclei isolation, and immunobloted against RAB18 antibody. Cytoplasmic (cyto) fractions were used for positive control. RAB18 is localized in the nuclei only of P25 animals.

Autophagic cargo of brain purified autophagosomes includes cytoskeletal and synaptic proteins

Previous work has described the autophagic cargo in yeast by proteomic profiling[109,110]. In mammalian tissues, mass spectrometry proteomic analyses from autophagosomes revealed great variety of weaknesses[111], while quantitative proteomics from human cells points the new way of analyzing autophagosome-related proteins[112,113]. The content of AVs, extracted from brain tissue, has recently been studied from our group[92], although without performing quantitative proteomic analyses. To make an effort towards this direction, AVs from forebrain of P25, P60 and P180 wild-type animals were purified with our established protocol, and further submitted to CE treatment. The isolated supernatant was analyzed, by Tandem Mass Spectrometry (MS/MS), using tandem mass tag (TMT) for quantitation (Proteomics Core Facility, EMBL, Heidelberg Germany). Purity of the extracted AVs, along with the verification of each isolated fraction and the success of the CE method, are determined by using specific markers (Figure S7). The results divulge a huge amount of proteins, classified in many categories, regarding their function and subcellular location (unpublished data). Two of the most interesting categories are cytoskeletal and synaptic proteins, especially in the age comparison P25-P180 (Figure 9A). Annotated proteins are classified to three groups; "HIT" corresponds to confident alteration of protein levels between P25 and P180, while "CANDIDATE" represents a possible protein level variation. "NO HIT" shows that the protein amount remains stable throughout the age comparison. To validate MS/MS proteomic analyses, Western blot analysis of the indicative proteins was performed in purified AVs of both ages, after CE treatment (Figure 9B). The established proteins are quantified with LC3B-II levels found in membranous pellet, after CE treatment of total AVs. As

expected, Synapsin 1 (Syn1), Synapsin 2 (Syn2) and Synaptojanin 1 (Synj1) levels were increased in P180 supernatant extracts. On the contrary, the remaining proteins demonstrate opposite outcomes in immunoblotted P180 supernatant samples; Parvalbumin (Pvalb), Calretinin (Calb2) and Cofilin 1 (CFL1) were found to be raised. Moreover, DLG3 amount was increased in P180 supernatants, failing to approve its stable levels coming from MS/MS analyses (Figure 9C). These incomparable outcomes may be attributed to the loading control that is used for experimental quantification. Essentially, LC3B-II, a member of Atg8 protein family, is the most well characterized marker of AVs, and has been widely used for monitoring and measuring autophagic activity[96]. However, in mammals, Atg8 family includes six protein members in total, divided to MAP1LC3 and GABARAP subfamilies. Indeed, we validated the existence of GABARAPL1 protein in forebrain tissue AVs, where its lipidated form is observed only in the AVs membranes (Figure S8). Therefore, a combination of AVs markers may be required for the correct experimental quantification.

A

Synapse - AVs P180-P25

Gene name	Protein name	Location	Annotation	Alteration
CALB2	Calretinin	Presynapse	HIT	Decreased in P180
PVALB	Parvalbumin alpha	Presynapse	HIT	Decreased in P180
SYN1	Synapsin-1	BOTH	HIT	Increased in P180
SYN2	Synapsin-2	BOTH	HIT	Increased in P180
CFL1	Cofilin-1	Postsynapse	CANDIDATE	Decreased in P180
SYNJ1	Synaptojanin-1	Presynapse	CANDIDATE	Increased in P180
DLG3	Disks large homolog 3	Postsynapse	NO HIT	Stable

Cytoskeleton - AVs P180-P25

Gene name	Protein name	Annotation	Alteration
SYN1	Synapsin-1	HIT	Increased in P180
CFL1	Cofilin-1	CANDIDATE	Decreased in P180
SYNJ1	Synaptojanin-1	CANDIDATE	Increased in P180
DLG3	Disks large homolog 3	NO HIT	Stable

B

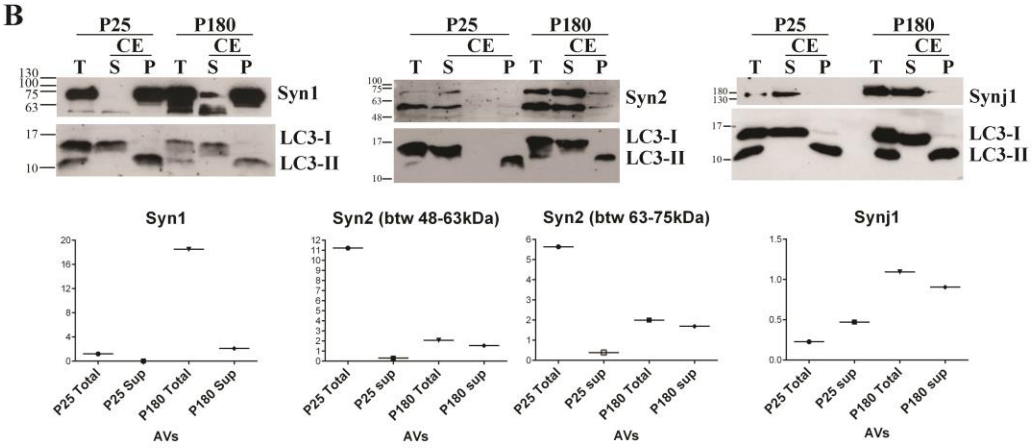

C

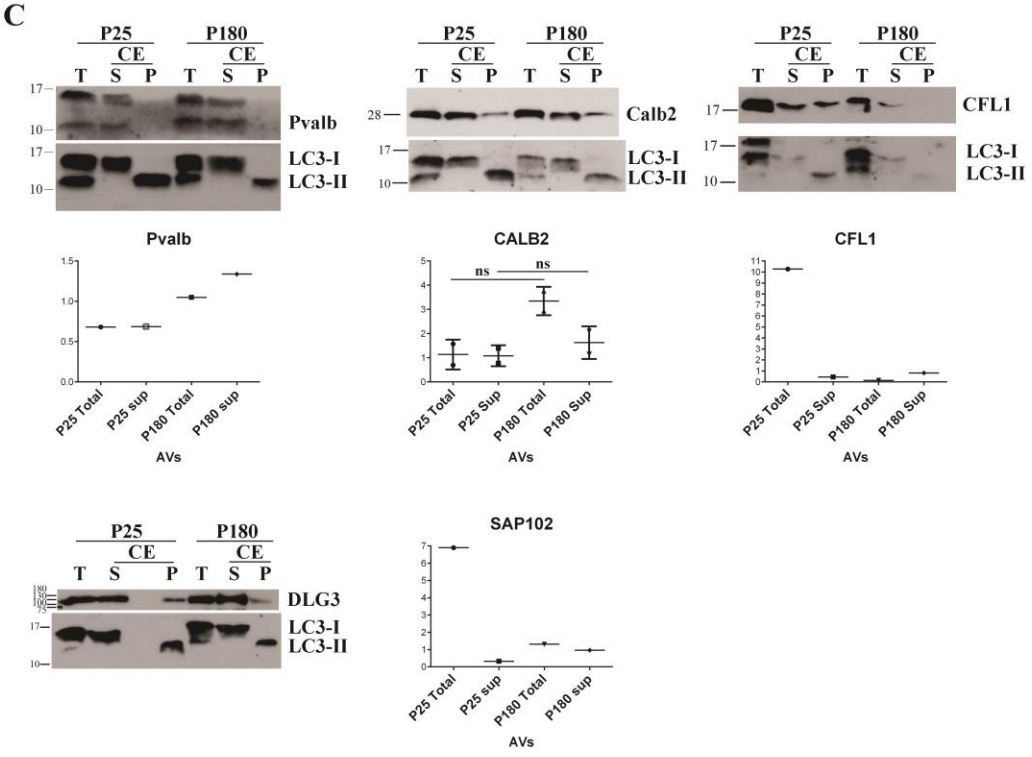

Figure 9 Validation of quantitative proteomic analyses verified the existence of synaptic and cytoskeletal proteins in the autophagosomal cargo

(A) Summary of major synaptic and cytoskeletal proteins, identified from Tandem quantitative proteomic analyses (MS/MS).
(B) AVs from indicated postnatal days, were fractionated to (S) and (P) by carbonate extraction and immunobloted against Syn1 (~75kD), Syn2 (two specific bands between 48-63kD and 63-75kD), Synj1 (~172kD). Graphs show the quantification. As loading control, LC3-II from (P) fraction was used for the (P) and (S) fractions, while LC3-II from (T) for the (T) fractions.
(C) Similarly to B, AVs from indicated postnatal days, were fractionated to (S) and (P) by carbonate extraction and immunobloted against Pvalb (12kD, non-specific at 15kD), Calb2 (~29kD), CFL1 (~19kD), SAP102/DLG3 (band btw 100-130kD). Graphs show the quantification. As loading control, LC3-II from (P) fraction was used for the (P) and (S) fractions, while LC3-II from (T) for the (T) fractions.
For all proteins except for Calb2, one experiment was performed. For Calb2 protein, two independent experiments were performed (N=2). When applied, statistical analysis was implemented by using unpaired Student's t test. From the statistical test, no statistical significance is reported. Graphs are representing by mean ± SD.

Ensuing the observation that proteins, clustered in specific families, are engulfed into the AVs, we set out to detect their respective levels in forebrain of P25 and P180 wild-type animals. As anticipated, protein quantities are reduced in P180 forebrain lysates, in line with our previous results of elevated quantities in P180 AVs supernatants (Figure 10A). Apart from forebrain lysates of wild-type, cortical lysates of control and *cAtg5* P25 animals were immunoblotted against the aforementioned antibodies (Figure 10B). Interestingly, all tested proteins present increased levels, suggesting that autophagy is a fundamental mechanism for the degradation of these protein clusters.

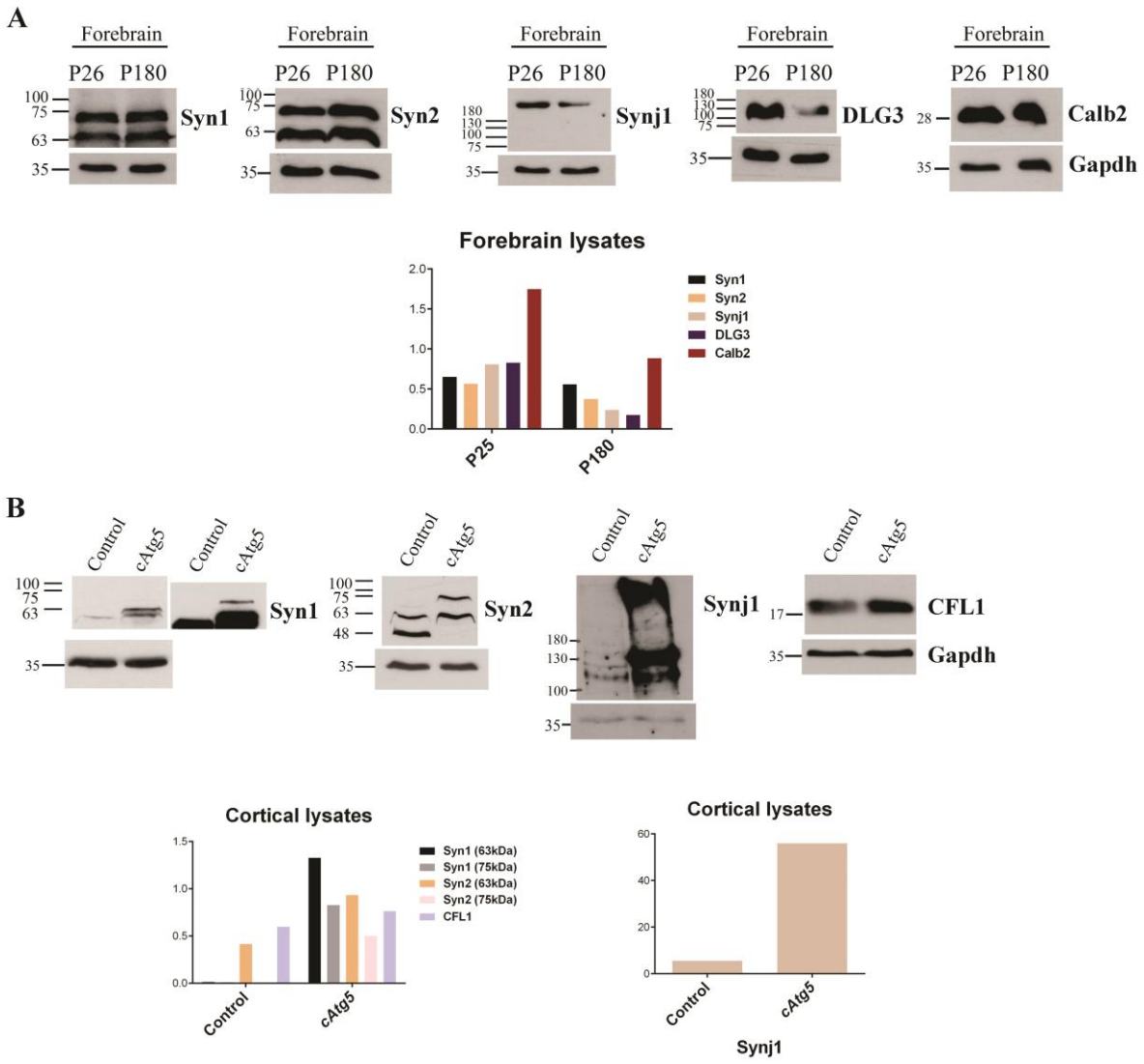

Figure 10 Identified synaptic and cytoskeletal proteins from proteomic analyses, express their levels in an age-dependent and *Atg5* dependent way, consisting to their possible cargo nature

(A) Forebrain lysates from indicative postnatal days of male animals were immunobloted against Syn1, Syn2, Synj1, SAP102/DLG3 and Calb2. As loading control, Gapdh was used. One experiment was performed.

(B) Forebrain lysates from P25 control (NestinCre;Atg5$^{+/+}$) or *cAtg5* animals were immunobloted against Syn1, Syn2, Sunj1 and CFL1. As loading control, Gapdh was used. One experiment was performed.

Discussion

Our work depicts the modulation of two LD markers by the autophagic machinery in the brain, providing the ground for speculations of how LDs are utilized from the central nervous system (CNS). These thesis findings strongly suggest that RAB18 acts as a positive modulator of autophagy in the nervous system, while PLIN2 acts as a substrate of autophagy, therefore enhancing lipophagy evidence in the brain. Chemical LTD reveals the positive regulation of RAB18 protein levels. Yet, it is elucidated that RAB18 is possible to associate to the biogenesis of AVs, as it is known that lipids hold a role in the AVs formation[54]. On top of that, l-PLIN2 acts as an autophagic cargo, since its amount is modulated in respect of increase or decline of autophagy. Likewise, stressor factors, for instance nutrient deprivation or oleic acid supply, further supported the aforementioned indications, as RAB18 and PLIN2 not only colocalize with LC3 and p62, but also represent critical elevated levels. Prolonged fasting periods lead to LD accumulation, in line with previous published work[98], where LDs biogenesis sequesters FA and assists the cell adaptation to lipotoxicity aroused by the hugely increase in autophagy. On the contrary, forebrain starved tissues, while they provided positive evidence for PLIN2 proposed function, failed to support RAB18 aforementioned results. Hence, we can speculate that RAB18 function may be regulated in a cell-type dependent manner, as glial cells contribute a considerable percentage to the physiology of the tissue. It is widely accepted that lipid biogenesis is substantial and of great importance in glial cells[114]. Oleic acid treatment in neuronal cultures, promotes the colocalization of RAB18 and PLIN2, an absent event in basal conditions, highlighting a possible altered role of these two proteins, under stress conditions. Approaching a more direct evidence of RAB18 and PLIN2 association with autophagy, only RAB18

functionally interacts with LC3 and p62 via its LIR motif, indicating that PLIN2 may require an intermediate interactor. Genetic ablation of *Atg5* gene in the neural lineage, further support our hypothesis for RAB18 and PLIN2 (s-PLIN2) functions, as their levels are diminished and enhanced respectively in three different brain regions; cortex, hippocampus and hypothalamus. The inconsistencies between the two "isoforms" of PLIN2 regarding their role in autophagic processes, may stem from low number of replicates. In addition, genetic ablation of *BDNF* gene in one allele in the neural lineage, leads to increase of RAB18 protein in cortical and cerebellum tissues, highlighting once more its positive modulator function. The ultimate confirmation of our hypothesis is the different localization of RAB18 and PLIN2 on the AV. RAB18 is localized exclusively in the pellet, whereas PLIN2 (both isoforms) exclusively in the supernatant. What is more, in enhanced autophagic circumstances, RAB18 and l-PLIN2 are increased in their specific location on the AV. All things consider, our data propose the existence of two different LD populations, with speculative different functions and roles in the brain, a notion supported by a previous study[57]. Certainly, there is evidence that LD proteome may determine the core content of the LD[115]. Notably, RAB18 has been previously implicated to play a role to lipogenesis and lipolysis in adipocytes[116]. Our findings link lipogenic RAB18 role in the forebrain, since it is located to the ER as well. Given the fact that lipolysis and lipophagy are commonly regulated[117], as they share a variety of transcription factors and genes, RAB18 role in lipophagy is more than clear. To our knowledge, this is the first report that supports RAB18 and PLIN2 roles in the CNS autophagic machinery. RAB18 dispose a trafficking role of LDs to ER with subsequent fusion after acute stress[118], and from ER to Golgi[119], while in a most recent study in the nervous system, RAB18 is implicated in secretion of sonic hedgehog (SHH) growth factor, as a core component of a distinct type of extracellular vesicles[120]. Taken all into account, our data allow us to

hypothesize that, apart from the degradation of LDs, autophagic machinery may facilitate lipid signaling within a neuronal cell and between neurons and glial cells.

Our established proteomic analyses in the supernatant of AVs, derived from forebrain of young (P25), early adults (P60) and mature animals (P180) determine distinct protein categories. Two protein subclasses that capture our attention, as a result of their strict connection to autophagy in the nervous system, are synaptic and cytoskeletal proteins. The studied postnatal days were selected on the basis of investigating the spine pruning (P20-P30), the early adulthood and the mature wiring of the brain. Mounting evidence points out the significance of autophagic machinery on maintaining synaptic transmission, as autophagy is indispensable both in presynaptic and postsynaptic sites[121]. In line with this information, our data shows that Synj1, Syn1, Syn2, Pvalb and Calb2 represent cargoes of the AV, which levels are considerably altered in the age comparison P25-P180. Synj1 has been described to regulate trafficking of synaptic vesicles, while Synj1 lipid phosphatase domain SAC1 is shown to be responsible for the AV formation in axon terminals[122]. Syn1 and Syn2 play a fundamental role in regulating neurotransmitter release, by coating synaptic vesicles to the cytoskeletal actin[123,124]. Pvalb has been described to modulate short term synaptic plasticity[125], whereas Calb2 is considered as a potent regulator of neuronal excitability[126]. Both proteins are core ingredients of distinct population of neurons[127]. Dlg3 protein is essential for the synapse development and plasticity, as a major component of glutamatergic synapses[128]. Moreover, it is a widely held view that cytoskeletal proteins modulate the autophagosome biogenesis, expansion and fusion with the lysosome, with actin, actomyosin, microtubule-associated proteins to play a major role[129]. Apart from this notion, F-actin (actin filaments) represents a critical synaptic structural constituent.

CFL1 has been characterized as a vital actin-depolymerization protein. Various evidence demonstrates that CFL1 affects the structure of dendritic spines, trafficking of glutamate receptors and synaptic plasticity[130]. The family of cofilins is hypothesized to influence the whole stage pathway of AV formation up to AV-lysosomal fusion, with published data to support the expansion stage[129]. Our proteomic analyses data invite us to speculate that autophagic machinery should be responsible for the selective sequestration of synaptic and cytoskeletal proteins and their regulation across maturation. The confirmation of their protein levels in wild-type forebrain lysates of respective ages and in *cAtg5* cortical lysates further support our hypothesis that, autophagy acts as a highly selective and regulatory mechanism of synaptic and cytoskeletal proteins during maturation.

Our findings, though they provide sufficient evidence for LDs role in CNS neurons, consist of one major weakness; the lack of direct proof that LDs role and signaling are impaired in neuronal autophagy depleted circumstances. One step closer towards this route, will be the isolation of LDs from the brain of control and *cAtg5* or *cBDNF* (BDNF is depleted in the neural lineage, in both alleles) animals and ascertain their proteome and core of lipids. Afterwards, in order to fully characterize lipid signaling in CNS, several approaches should be followed, in the base of out identification of different LD populations. For example, it should be developed a method of distinguishing the different LD species, based on their proteome and subsequent access their lipid core content. What is more, since lipophagy and lipolysis represent two sides of the same coin[117], lipolysis should be monitored in parallel. On the same notion, CMA should also be accessed simultaneously, since a clear crosstalk and influence between CMA and autophagy has been established[131]. Investigating the transcriptional regulation of RAB18 and PLIN2 is the CNS

will be an additional asset in our effort. Lipidomic analysis of the isolated AVs will show the different lipid species between young and mature brains, indicating the role of lipid signaling. Furthermore, for safely identify and characterize the nature of autophagosomal cargo, lysosomal isolation should be employed, in order to verify that lysosomes are the final destination of cargoes. Additionally, electron microscopy experiments should be performed, for the verification of AVs purity, colocalization of cargoes with AV markers, such as LC3-II, and the identification of LDs in the brain. Lastly, lysosomal and proteasomal activities should be also studied in the context of forebrain maturation, since there is a huge amount of evidence that connect autophagy with the ubiquitin-proteasome machinery[132].

References

1. Tsukada, M. & Ohsumi, Y. Isolation and characterization of autophagy-defective mutants of Saccharomyces cerevisiae. *FEBS Lett.* **333,** 169–74 (1993).

2. De Duve, C. & Wattiaux, R. Functions of lysosomes. *Annu. Rev. Physiol.* **28,** 435–92 (1966).

3. Yang, Z. & Klionsky, D. J. Eaten alive: a history of macroautophagy. *Nat. Cell Biol.* **12,** 814–822 (2010).

4. Galluzzi, L. *et al.* Molecular definitions of autophagy and related processes. *EMBO J.* **36,** 1811–1836 (2017).

5. Dice, J. F. Peptide sequences that target cytosolic proteins for lysosomal proteolysis. *Trends Biochem. Sci.* **15,** 305–9 (1990).

6. Kaushik, S. & Cuervo, A. M. Chaperone-mediated autophagy: a unique way to enter the lysosome world. *Trends Cell Biol.* **22,** 407–417 (2012).

7. Kaushik, S. & Cuervo, A. M. Degradation of lipid droplet-associated proteins by chaperone-mediated autophagy facilitates lipolysis. *Nat. Cell Biol.* **17,** 759–70 (2015).

8. Marzella, L., Ahlberg, J. & Glaumann, H. Autophagy, heterophagy, microautophagy and crinophagy as the means for intracellular degradation. *Virchows Arch. B. Cell Pathol. Incl. Mol. Pathol.* **36,** 219–34 (1981).

9. Vevea, J. D. *et al.* Role for Lipid Droplet Biogenesis and Microlipophagy in Adaptation to Lipid Imbalance in Yeast. *Dev. Cell* **35,** 584–599 (2015).

10. Seo, A. Y. *et al.* AMPK and vacuole-associated Atg14p orchestrate μ-lipophagy for energy production and long-term survival under glucose starvation. *Elife* **6,** (2017).

11. Lemasters, J. J. Variants of mitochondrial autophagy: Types 1 and 2 mitophagy and micromitophagy (Type 3). *Redox Biol.* **2,** 749–754 (2014).

12. Tekirdag, K. & Cuervo, A. M. Chaperone-mediated autophagy and endosomal microautophagy: Joint by a chaperone. *J. Biol. Chem.* **293,** 5414–5424 (2018).

13. Yu, L., Chen, Y. & Tooze, S. A. Autophagy pathway: Cellular and molecular mechanisms. *Autophagy* **14,** 207–215 (2018).

14. Axe, E. L. *et al.* Autophagosome formation from membrane compartments enriched in phosphatidylinositol 3-phosphate and dynamically connected to the endoplasmic reticulum. *J. Cell Biol.* **182,** 685–701 (2008).

15. Biazik, J., Ylä-Anttila, P., Vihinen, H., Jokitalo, E. & Eskelinen, E.-L. Ultrastructural relationship of the phagophore with surrounding organelles. *Autophagy* **11,** 439–51 (2015).

16. Karanasios, E. *et al.* Autophagy initiation by ULK complex assembly on ER tubulovesicular regions marked by ATG9 vesicles. *Nat. Commun.* **7,** 1–17 (2016).

17. Ganley, I. G. *et al.* ULK1·ATG13·FIP200 Complex Mediates mTOR Signaling and Is Essential for Autophagy. *J. Biol. Chem.* **284,** 12297–12305 (2009).

18. Mercer, C. A., Kaliappan, A. & Dennis, P. B. A novel, human Atg13 binding protein, Atg101, interacts with ULK1 and is essential for macroautophagy. *Autophagy* **5,** 649–62 (2009).

19. Hosokawa, N. *et al.* Atg101, a novel mammalian autophagy protein interacting with Atg13. *Autophagy* **5,** 973–9 (2009).

20. Papinski, D. *et al.* Early Steps in Autophagy Depend on Direct Phosphorylation of Atg9 by the Atg1 Kinase. *Mol. Cell* **53,** 471–483 (2014).

21. Lamb, C. A., Yoshimori, T. & Tooze, S. A. The autophagosome: origins unknown, biogenesis complex. *Nat. Rev. Mol. Cell Biol.* **14,** 759–774 (2013).

22. Itakura, E., Kishi, C., Inoue, K. & Mizushima, N. Beclin 1 Forms Two Distinct Phosphatidylinositol 3-Kinase Complexes with Mammalian Atg14 and UVRAG. *Mol. Biol. Cell* **19,** 5360–5372 (2008).

23. Zhong, Y. *et al.* Distinct regulation of autophagic activity by Atg14L and Rubicon associated with Beclin 1–phosphatidylinositol-3-kinase complex. *Nat. Cell Biol.* **11,** 468–476 (2009).

24. Weidberg, H., Shvets, E. & Elazar, Z. Biogenesis and Cargo Selectivity of Autophagosomes. *Annu. Rev. Biochem.* **80,** 125–156 (2011).

25. Proikas-Cezanne, T., Takacs, Z., Donnes, P. & Kohlbacher, O. WIPI proteins: essential PtdIns3P effectors at the nascent autophagosome. *J. Cell Sci.* **128,** 207–217 (2015).

26. Geng, J. & Klionsky, D. J. The Atg8 and Atg12 ubiquitin-like conjugation systems in macroautophagy. 'Protein Modifications: Beyond the Usual Suspects' Review Series. *EMBO Rep.* **9,** 859–864 (2008).

27. Jung, C. H., Ro, S.-H., Cao, J., Otto, N. M. & Kim, D.-H. mTOR regulation of autophagy. *FEBS Lett.* **584,** 1287–1295 (2010).

28. Sancak, Y. *et al.* Ragulator-Rag Complex Targets mTORC1 to the Lysosomal Surface and Is Necessary for Its Activation by Amino Acids. *Cell* **141,** 290–303 (2010).

29. Bar-Peled, L., Schweitzer, L. D., Zoncu, R. & Sabatini, D. M. Ragulator Is a GEF for the Rag GTPases that Signal Amino Acid Levels to mTORC1. *Cell* **150,** 1196–1208 (2012).

30. Kim, J., Kundu, M., Viollet, B. & Guan, K.-L. AMPK and mTOR regulate autophagy through direct phosphorylation of Ulk1. *Nat. Cell Biol.* **13,** 132–141 (2011).

31. Djouder, N. *et al.* PKA phosphorylates and inactivates AMPKα to promote efficient lipolysis. *EMBO J.* **29,** 469–481 (2010).

32. Shaw, R. J. LKB1 and AMP-activated protein kinase control of mTOR signalling and growth. *Acta Physiol.* **196,** 65–80 (2009).

33. Settembre, C. *et al.* TFEB Links Autophagy to Lysosomal Biogenesis. *Science (80-.).* **332,** 1429–1433 (2011).

34. Koga, H., Kaushik, S. & Cuervo, A. M. Altered lipid content inhibits autophagic vesicular fusion. *FASEB J.* **24,** 3052–3065 (2010).

35. Las, G., Serada, S. B., Wikstrom, J. D., Twig, G. & Shirihai, O. S. Fatty Acids Suppress Autophagic Turnover in β-Cells. *J. Biol. Chem.* **286,** 42534–42544 (2011).

36. Choi, S.-E. *et al.* Protective Role of Autophagy in Palmitate-Induced INS-1 β-Cell Death. *Endocrinology* **150,** 126–134 (2009).

37. Komiya, K. *et al.* Free fatty acids stimulate autophagy in pancreatic β-cells via JNK pathway. *Biochem. Biophys. Res. Commun.* **401,** 561–567 (2010).

38. Farré, J. C. & Subramani, S. Mechanistic insights into selective autophagy pathways: Lessons from yeast. *Nat. Rev. Mol. Cell Biol.* **17,** 537–552 (2016).

39. Gatica, D., Lahiri, V. & Klionsky, D. J. Cargo recognition and degradation by selective autophagy. *Nat. Cell Biol.* **20,** 233–242 (2018).

40. Isakson, P., Holland, P. & Simonsen, A. The role of ALFY in selective autophagy. *Cell Death Differ.* **20,** 12–20 (2013).

41. Katsuragi, Y., Ichimura, Y. & Komatsu, M. p62/SQSTM1 functions as a signaling hub and an autophagy adaptor. *FEBS J.* **282,** 4672–4678 (2015).

42. A˚ sa Birna, B., Trond, L. & Terje, J. The LIR motif – crucial for selective autophagy. *J. Cell Sci.* **126,** 3237–3247 (2013).

43. Anding, A. L. & Baehrecke, E. H. Cleaning House: Selective Autophagy of Organelles. *Dev. Cell* **41,** 10–22 (2017).

44. Cudjoe, E. K., Saleh, T., Hawkridge, A. M. & Gewirtz, D. A. Proteomics Insights into Autophagy. *Proteomics* **17,** (2017).

45. Ward, C. *et al.* Autophagy, lipophagy and lysosomal lipid storage disorders. *Biochim. Biophys. Acta - Mol. Cell Biol. Lipids* **1861,** 269–284 (2016).

46. Schulze, R. J., Sathyanarayan, A. & Mashek, D. G. Breaking fat: The regulation and mechanisms of lipophagy. *Biochim. Biophys. Acta - Mol. Cell Biol. Lipids* (2017). doi:10.1016/j.bbalip.2017.06.008

47. Singh, R. *et al.* Autophagy regulates lipid metabolism. *Nature* **458,** 1131–5 (2009).

48. Onal, G., Kutlu, O., Gozuacik, D. & Dokmeci Emre, S. Lipid Droplets in Health and Disease. *Lipids Health Dis.* **16,** 128 (2017).

49. O'Byrne, S. M. & Blaner, W. S. Retinol and retinyl esters: biochemistry and physiology. *J. Lipid Res.* **54,** 1731–1743 (2013).

50. Gluchowski, N. L., Becuwe, M., Walther, T. C. & Farese, R. V. Lipid droplets and liver disease: from basic biology to clinical implications. *Nat. Rev. Gastroenterol. Hepatol.* **14,** 343–355 (2017).

51. Thiele, C. & Spandl, J. Cell biology of lipid droplets. *Curr. Opin. Cell Biol.* **20,** 378–385 (2008).

52. Kory, N., Farese, R. V. & Walther, T. C. Targeting Fat: Mechanisms of Protein Localization to Lipid Droplets. *Trends Cell Biol.* **26,** 535–546 (2016).

53. Ohsaki, Y. *et al.* PML isoform II plays a critical role in nuclear lipid droplet formation. *J. Cell Biol.* **212,** 29–38 (2016).

54. Shpilka, T. *et al.* Lipid droplets and their component triglycerides and steryl esters regulate autophagosome biogenesis. *EMBO J.* **34,** 2117–2131 (2015).

55. Carlsson, S. R. & Simonsen, A. Membrane dynamics in autophagosome biogenesis. *J. Cell Sci.* **128,** 193–205 (2015).

56. Name, L. *et al.* Quantitative analysis of the murine lipid droplet-associated proteome during diet-induced hepatic steatosis. *Igarss 2014* **56,** 1–5 (2014).

57. Ozeki, S. Rab18 localizes to lipid droplets and induces their close apposition to the

endoplasmic reticulum-derived membrane. *J. Cell Sci.* **118,** 2601–2611 (2005).

58. Bento, C. F., Puri, C., Moreau, K. & Rubinsztein, D. C. The role of membrane-trafficking small GTPases in the regulation of autophagy. *J. Cell Sci.* **126,** 1059–1069 (2013).

59. Gerondopoulos, A. *et al.* Rab18 and a Rab18 GEF complex are required for normal ER structure. *J. Cell Biol.* **205,** 707–720 (2014).

60. Li, C. *et al.* COPI–TRAPPII activates Rab18 and regulates its lipid droplet association. *EMBO J.* **36,** 441–457 (2017).

61. Xu, D. *et al.* Rab18 promotes lipid droplet (LD) growth by tethering the ER to LDs through SNARE and NRZ interactions. *J. Cell Biol.* jcb.201704184 (2018). doi:10.1083/jcb.201704184

62. Kiss, R. S. & Nilsson, T. Rab proteins implicated in lipid storage and mobilization. *J. Biomed. Res.* (2014). doi:10.7555/JBR.28.20140029

63. Martin, S., Driessen, K., Nixon, S. J., Zerial, M. & Parton, R. G. Regulated localization of Rab18 to lipid droplets: Effects of lipolytic stimulation and inhibition of lipid droplet catabolism. *J. Biol. Chem.* **280,** 42325–42335 (2005).

64. Schulze, R. J., Drižytė, K., Casey, C. A. & McNiven, M. A. Hepatic lipophagy: New insights into autophagic catabolism of lipid droplets in the liver. *Hepatol. Commun.* **1,** 359–369 (2017).

65. Feldmann, A. *et al.* The RAB GTPase RAB18 modulates macroautophagy and proteostasis. *Biochem. Biophys. Res. Commun.* **486,** 738–743 (2017).

66. Spang, N. *et al.* RAB3GAP1 and RAB3GAP2 modulate basal and rapamycin-induced autophagy. *Autophagy* **10,** 2297–2309 (2014).

67. Kern, A. *et al.* RAB18 impacts autophagy via lipid droplet-derived lipid transfer and is rescued by ATG9A. *BioRχiv* (2018). doi:10.1101/421677

68. Jayson, C. B. K. *et al.* Rab18 is not necessary for lipid droplet biogenesis or turnover in human mammary carcinoma cells. *Mol. Biol. Cell* **29,** 2045–2054 (2018).

69. Bickel, P. E., Tansey, J. T. & Welte, M. A. PAT proteins, an ancient family of lipid droplet proteins that regulate cellular lipid stores. *Biochim. Biophys. Acta* **1791,** 419–40 (2009).

70. Rowe, E. R. *et al.* Conserved Amphipathic Helices Mediate Lipid Droplet Targeting of Perilipins 1–3. *J. Biol. Chem.* **291,** 6664–6678 (2016).

71. Soni, K. G. *et al.* Coatomer-dependent protein delivery to lipid droplets. *J. Cell Sci.* **122,** 1834–1841 (2009).

72. Robenek, H. *et al.* Adipophilin-enriched domains in the ER membrane are sites of lipid droplet biogenesis. *J. Cell Sci.* **119,** 4215–4224 (2006).

73. Xu, S., Zhang, X. & Liu, P. Lipid droplet proteins and metabolic diseases. *Biochim. Biophys. Acta - Mol. Basis Dis.* **1864,** 1968–1983 (2018).

74. Smirnova, E. *et al.* ATGL has a key role in lipid droplet/adiposome degradation in mammalian cells. *EMBO Rep.* **7,** 106–113 (2006).

75. Sathyanarayan, A., Mashek, M. T. & Mashek, D. G. ATGL Promotes Autophagy/Lipophagy via SIRT1 to Control Hepatic Lipid Droplet Catabolism. *Cell Rep.* **19,** 1–9 (2017).

76. Itabe, H., Yamaguchi, T., Nimura, S. & Sasabe, N. Perilipins: a diversity of intracellular lipid droplet proteins. *Lipids Health Dis.* **16,** 83 (2017).

77. Takahashi, Y. *et al.* Perilipin2 plays a positive role in adipocytes during lipolysis by escaping proteasomal degradation. *Sci. Rep.* **6,** 20975 (2016).

78. Nguyen, K. T. *et al.* N-terminal acetylation and the N-end rule pathway control degradation of the lipid droplet protein PLIN2. *J. Biol. Chem.* jbc.RA118.005556 (2018). doi:10.1074/jbc.RA118.005556

79. Kaushik, S. & Cuervo, A. M. Degradation of lipid droplet-associated proteins by chaperone-mediated autophagy facilitates lipolysis. *Nat. Cell Biol.* **17,** 759–770 (2015).

80. Kaushik, S. & Cuervo, A. M. AMPK-dependent phosphorylation of lipid droplet protein PLIN2 triggers its degradation by CMA. *Autophagy* **12,** 432–438 (2016).

81. Tsai, T.-H. *et al.* The constitutive lipid droplet protein PLIN2 regulates autophagy in liver. *Autophagy* **13,** 1130–1144 (2017).

82. Rapoport, S. I., Chang, M. C. & Spector, A. A. Delivery and turnover of plasma-derived essential PUFAs in mammalian brain. *J. Lipid Res.* **42,** 678–85 (2001).

83. Ebert, D., Haller, R. G. & Walton, M. E. Energy Contribution of Octanoate to Intact Rat Brain Metabolism Measured by 13 C Nuclear Magnetic Resonance Spectroscopy. *J. Neurosci.* **23,** 5928–5935 (2003).

84. Tracey, T. J., Steyn, F. J., Wolvetang, E. J. & Ngo, S. T. Neuronal Lipid Metabolism: Multiple Pathways Driving Functional Outcomes in Health and Disease. *Front. Mol. Neurosci.* **11,** 1–25 (2018).

85. Bazinet, R. P. & Layé, S. Polyunsaturated fatty acids and their metabolites in brain function and disease. *Nat. Rev. Neurosci.* **15,** 771–785 (2014).

86. Shamim, A., Mahmood, T., Ahsan, F., Kumar, A. & Bagga, P. Lipids: An insight into the neurodegenerative disorders. *Clin. Nutr. Exp.* **20,** 1–19 (2018).

87. Martinez-Vicente, M. *et al.* Cargo recognition failure is responsible for inefficient autophagy in Huntington's disease. *Nat. Neurosci.* **13,** 567–576 (2010).

88. Kaushik, S. *et al.* Autophagy in hypothalamic agrp neurons regulates food intake and energy balance. *Cell Metab.* **14,** 173–183 (2011).

89. Tatsumi, T. *et al.* Forced lipophagy reveals that lipid droplets are required for early embryonic development in mouse. *Development* **145,** dev161893 (2018).

90. Hara, T. *et al.* Suppression of basal autophagy in neural cells causes neurodegenerative disease in mice. *Nature* **441,** 885–889 (2006).

91. Spijker, S. in 13–26 (2011). doi:10.1007/978-1-61779-111-6_2

92. Nikoletopoulou, V., Sidiropoulou, K., Kallergi, E., Dalezios, Y. & Tavernarakis, N. Modulation of Autophagy by BDNF Underlies Synaptic Plasticity. *Cell Metab.* **26,** 230–242.e5 (2017).

93. Singh, R. *et al.* Autophagy regulates lipid metabolism. *Nature* **458,** 1131–1135 (2009).

94. Durandt, C. *et al.* Novel flow cytometric approach for the detection of adipocyte subpopulations during adipogenesis. *J. Lipid Res.* **57,** 729–742 (2016).

95. Kalvari, I. *et al.* iLIR: A web resource for prediction of Atg8-family interacting proteins. *Autophagy* **10,** 913–25 (2014).

96. Klionsky, D. J. *et al.* Guidelines for the use and interpretation of assays for monitoring autophagy (3rd edition). *Autophagy* **12,** 1–222 (2016).

97. Young, J. E., Martinez, R. A. & La Spada, A. R. Nutrient Deprivation Induces Neuronal Autophagy and Implicates Reduced Insulin Signaling in Neuroprotective Autophagy Activation. *J. Biol. Chem.* **284,** 2363–2373 (2009).

98. Nguyen, T. B. *et al.* DGAT1-Dependent Lipid Droplet Biogenesis Protects Mitochondrial Function during Starvation-Induced Autophagy. *Dev. Cell* **42,** 9–21.e5 (2017).

99. Egan, D. F. *et al.* Small Molecule Inhibition of the Autophagy Kinase ULK1 and Identification of ULK1 Substrates. *Mol. Cell* **59,** 285–297 (2015).

100. Korte, M. *et al.* Hippocampal long-term potentiation is impaired in mice lacking brain-derived neurotrophic factor. *Proc. Natl. Acad. Sci.* **92,** 8856–8860 (1995).

101. Revest, J.-M. *et al.* BDNF-TrkB signaling through Erk1/2MAPK phosphorylation mediates the enhancement of fear memory induced by glucocorticoids. *Mol. Psychiatry*

19, 1001–1009 (2014).

102. Suzuki, S. *et al.* Brain-Derived Neurotrophic Factor Regulates Cholesterol Metabolism for Synapse Development. **27,** 6417–6427 (2007).

103. Collingridge, G. L., Peineau, S., Howland, J. G. & Wang, Y. T. Long-term depression in the CNS. *Nat. Rev. Neurosci.* **11,** 459–473 (2010).

104. Bingol, B. & Sheng, M. Deconstruction for Reconstruction: The Role of Proteolysis in Neural Plasticity and Disease. *Neuron* **69,** 22–32 (2011).

105. Shehata, M., Matsumura, H., Okubo-Suzuki, R., Ohkawa, N. & Inokuchi, K. Neuronal Stimulation Induces Autophagy in Hippocampal Neurons That Is Involved in AMPA Receptor Degradation after Chemical Long-Term Depression. *J. Neurosci.* **32,** 10413–10422 (2012).

106. Hou, L. & Klann, E. Activation of the phosphoinositide 3-kinase-Akt-mammalian target of rapamycin signaling pathway is required for metabotropic glutamate receptor-dependent long-term depression. *J. Neurosci.* **24,** 6352–61 (2004).

107. Antion, M. D., Hou, L., Wong, H., Hoeffer, C. A. & Klann, E. mGluR-Dependent Long-Term Depression Is Associated with Increased Phosphorylation of S6 and Synthesis of Elongation Factor 1A but Remains Expressed in S6K-Deficient Mice. *Mol. Cell. Biol.* **28,** 2996–3007 (2008).

108. Farese, R. V. & Walther, T. C. Lipid droplets go nuclear. *J. Cell Biol.* **212,** 7–8 (2016).

109. Dengjel, J. *et al.* Identification of Autophagosome-associated Proteins and Regulators by Quantitative Proteomic Analysis and Genetic Screens. *Mol. Cell. Proteomics* **11,** M111.014035 (2012).

110. Suzuki, K. *et al.* Proteomic Profiling of Autophagosome Cargo in Saccharomyces cerevisiae. *PLoS One* **9,** e91651 (2014).

111. Øverbye, A., Fengsrud, M. & Seglen, P. O. Proteomic analysis of membrane-associated proteins from rat liver autophagosomes. *Autophagy* **3,** 300–22

112. Mancias, J. D., Wang, X., Gygi, S. P., Harper, J. W. & Kimmelman, A. C. Quantitative proteomics identifies NCOA4 as the cargo receptor mediating ferritinophagy. *Nature* **509,** 105–109 (2014).

113. Zhang, T., Shen, S., Qu, J. & Ghaemmaghami, S. Global Analysis of Cellular Protein Flux Quantifies the Selectivity of Basal Autophagy. *Cell Rep.* **14,** 2426–2439 (2016).

114. Montani, L. & Suter, U. Building lipids for myelin. *Aging (Albany. NY).* **10,** 861–862 (2018).

115. Thiam, A. R. & Beller, M. The why, when and how of lipid droplet diversity. *J. Cell Sci.* **130,** 315–324 (2017).

116. Pulido, M. R. *et al.* Rab18 Dynamics in Adipocytes in Relation to Lipogenesis, Lipolysis and Obesity. *PLoS One* **6,** e22931 (2011).

117. Zechner, R., Madeo, F. & Kratky, D. Cytosolic lipolysis and lipophagy: two sides of the same coin. *Nat. Publ. Gr.* (2017). doi:10.1038/nrm.2017.76

118. Makino, A. *et al.* Acute accumulation of free cholesterol induces the degradation of perilipin 2 and Rab18-dependent fusion of ER and lipid droplets in cultured human hepatocytes. *Mol. Biol. Cell* **27,** 3293–3304 (2016).

119. Dejgaard, S. Y. *et al.* Rab18 and Rab43 have key roles in ER-Golgi trafficking. *J. Cell Sci.* **121,** 2768–2781 (2008).

120. Coulter, M. E. *et al.* The ESCRT-III Protein CHMP1A Mediates Secretion of Sonic Hedgehog on a Distinctive Subtype of Extracellular Vesicles. *Cell Rep.* **24,** 973–986.e8 (2018).

121. Nikoletopoulou, V. & Tavernarakis, N. Regulation and Roles of Autophagy at Synapses. *Trends Cell Biol.* **28,** 646–661 (2018).

122. Vanhauwaert, R. *et al.* The SAC1 domain in synaptojanin is required for autophagosome maturation at presynaptic terminals. *EMBO J.* **36,** 1392–1411 (2017).

123. Cesca, F., Baldelli, P., Valtorta, F. & Benfenati, F. The synapsins: Key actors of synapse function and plasticity. *Prog. Neurobiol.* **91,** 313–348 (2010).

124. Sang-Ho, S. & Augustine, G. J. Synapsin Isoforms and Synaptic Vesicle Trafficking. *Mol. Cells* **38,** 936–940 (2015).

125. Caillard, O. *et al.* Role of the calcium-binding protein parvalbumin in short-term synaptic plasticity. *Proc. Natl. Acad. Sci.* **97,** 13372–13377 (2000).

126. Camp, A. J. & Wijesinghe, R. Calretinin: Modulator of neuronal excitability. *Int. J. Biochem. Cell Biol.* **41,** 2118–2121 (2009).

127. Gulyás, A. I., Hájos, N. & Freund, T. F. Interneurons Containing Calretinin Are Specialized to Control Other Interneurons in the Rat Hippocampus. *J. Neurosci.* **16,** 3397–3411 (1996).

128. Crocker-Buque, A. *et al.* Altered thalamocortical development in the SAP102 knockout model of intellectual disability. *Hum. Mol. Genet.* **25,** 4052–4061 (2016).

129. Kast, D. J. & Dominguez, R. The Cytoskeleton–Autophagy Connection. *Curr. Biol.* **27,** R318–R326 (2017).

130. Rust, M. B. Novel functions for ADF/cofilin in excitatory synapses - lessons from gene-targeted mice. *Commun. Integr. Biol.* **8,** e1114194 (2015).

131. Wang, C. *et al.* Phosphorylation of ULK1 affects autophagosome fusion and links chaperone-mediated autophagy to macroautophagy. *Nat. Commun.* **9,** (2018).

132. Hoon Ji, C. & Yong Tae, K. Crosstalk and Interplay between the Ubiquitin-Proteasome System and Autophagy. *Mol. Cells* (2017). doi:10.14348/molcells.2017.0115

Appendix

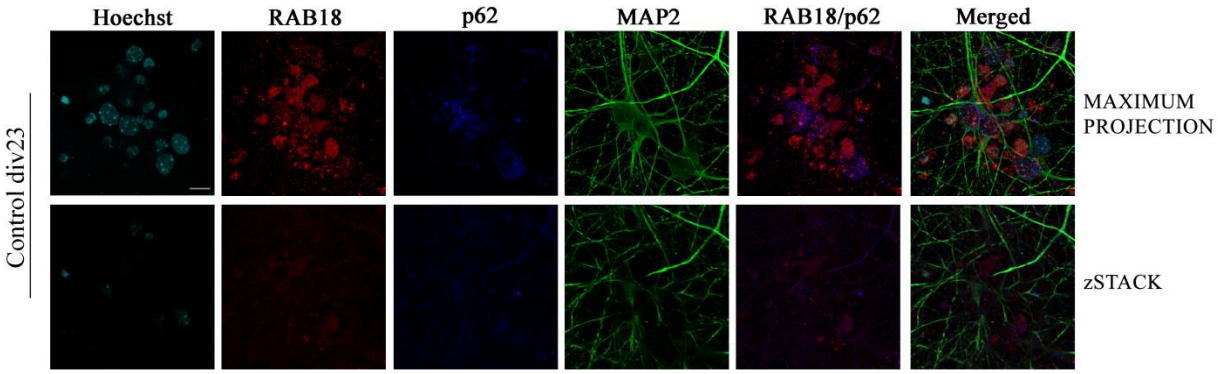

Figure S1 RAB18 do not colocalize with p62 in basal conditions
Cortical cultured neurons, *div23*, were immunostained against RAB18, p62 and MAP2 antibodies, while dyed with the nuclear marker Hoechst. There was not observed any colocalization of RAB18 and p62.
Scale bar=10µm. Maximum projection of z-Stacks or z-Stacks representation is indicated in each image panel.

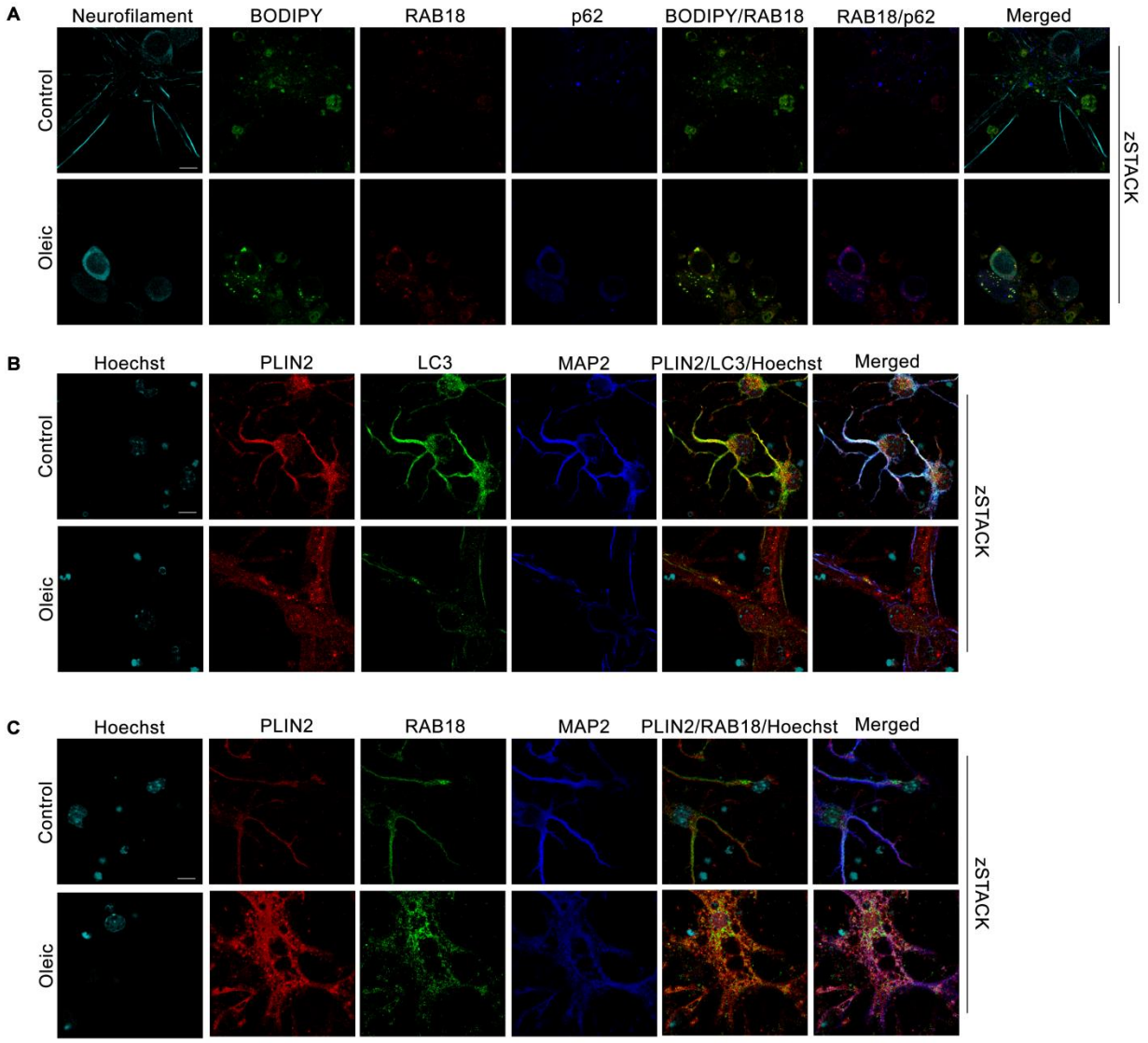

Figure S2 Oleic acid treatment significantly promotes the colocalization of RAB and PLIN2 with autophagic markers, whereas RAB18 and PLIN2 colocalization is also observed

(A) Cortical cultured neurons, *div21*, were treated with oleic acid (250μM) for 4 hours and immunostained against RAB18, p62, MAP2 and Neurofilament, while they also dyed with BODIPY493/503. Extreme colocalization and punctated signal of RAB18, BODIPY493/503 and p62 is observed.

(B) Similarly to A, cortical cultured neurons, *div21*, were treated with oleic acid (250μM) for 4 hours and immunostained against PLIN2, LC3 and MAP2, while they also dyed with BODIPY493/503 and Hoechst. Extreme colocalization and punctated signal of PLIN2, BODIPY493/503 and LC3 is observed.

(C) Cortical cultured neurons, *div21*, were treated with oleic acid (250μM) for 4 hours and immunostained against RAB18, PLIN2 and MAP2, while they also dyed with Hoechst. Extreme colocalization and punctated signal of RAB18 and PLIN2 is observed.

Scale bar=10μm. Images from z-Stacks are presented.

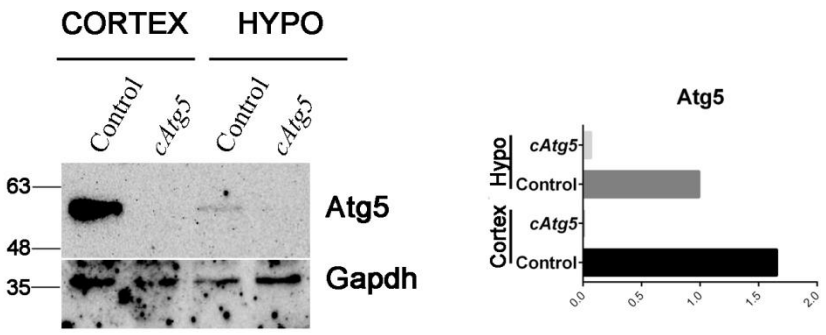

Figure S3 *Atg5* gene is conditionally ablated in cortex and hypothalamus of P25 male animals
Cortical and hypothalamic lysates from control (noCre;Atg5 $^{f/f}$) and *cAtg5* animals were immunobloted against Atg5 (~57kD). As loading control Gapdh is used. The graph represents the quantification.

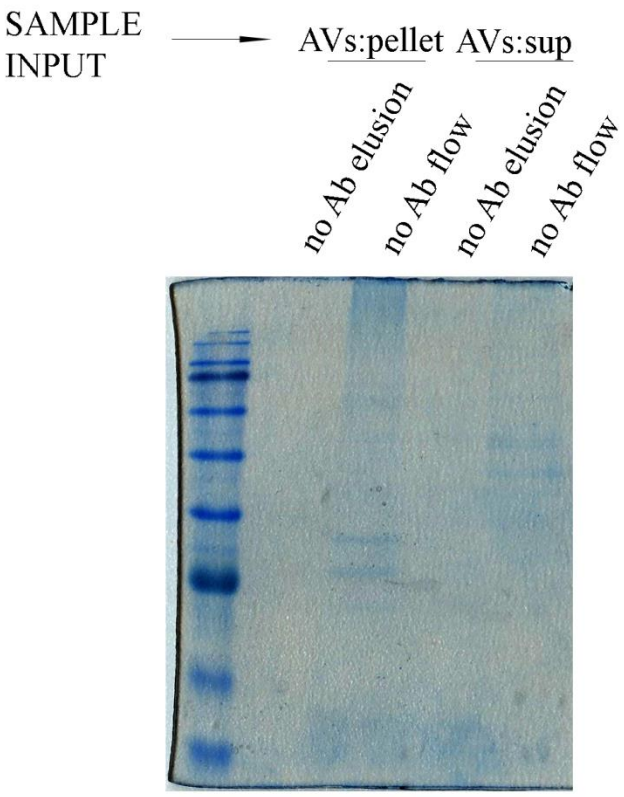

Figure S4 Positive control of immunoprecipiotation experiment at Figure 7C
Immunoprecipitation of no antibody-conjugated beads, using as sample input (P) or (S) AVs fractions and subsequent staining with Coomassie Blue dye, to verify the results of Figure 7C.

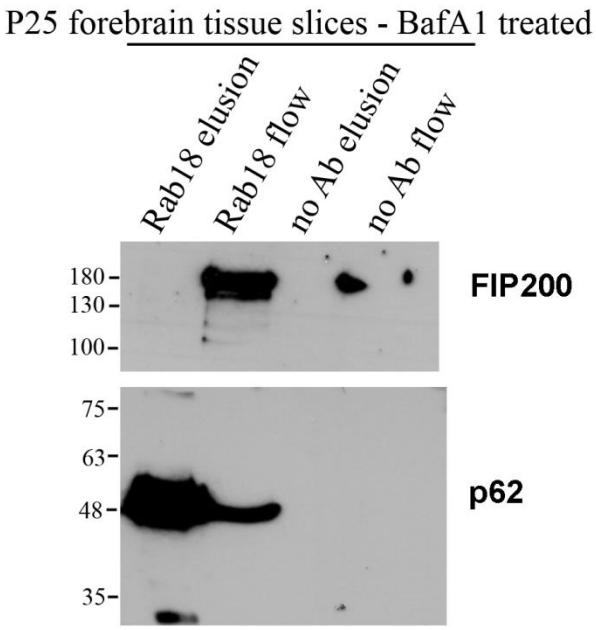

Figure S5 RAB18 does not interact with FIP200
Immunoprecipitation of RAB18-conjugated beads, using as sample input ex vivo forebrain treated slices with Baf A1 (10nM) for three hours, and subsequent immunobloted for FIP200 (~180kD). RAB18 does not appear to ineract with FIP200. The experiment should be repeated, as p62 gave a negative result, indicating that this experiment may not have been successful.

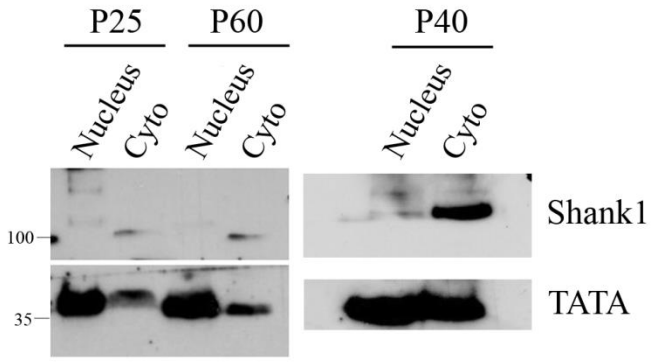

Figure S6 Positive control of purified nuclei with cytoplasmic and nuclear markers
Forebrains from male animals of indicative postnatal days were submitted to nuclei isolation, and immunobloted against cytoplasmic marker (Shank1) and nuclear marker (TATA - ~35kD). The purity of nuclei isolation is determined. [This experiment was performed by Akrivi-Dimitra Daskalaki, MSc]

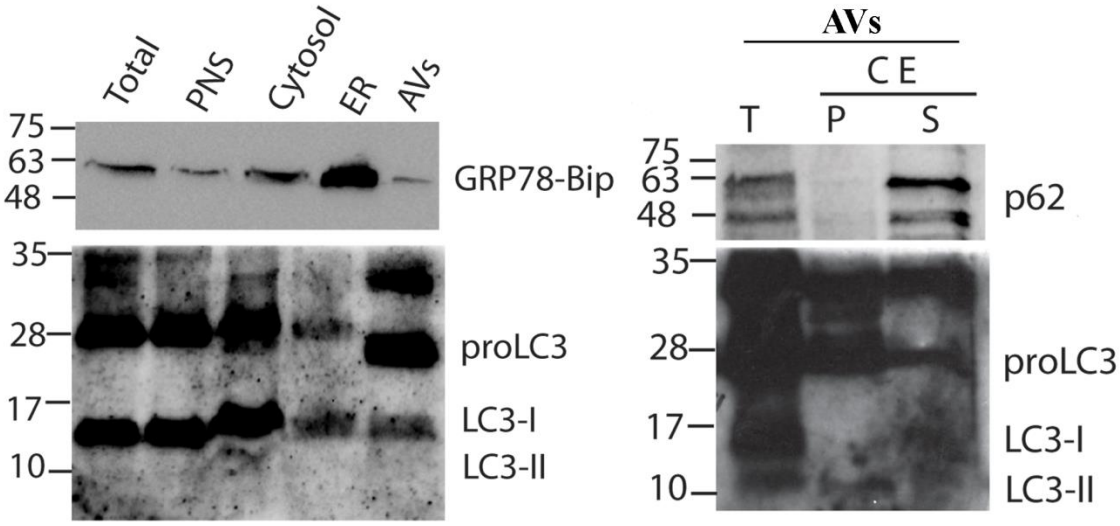

Figure S7 Purity of the extracted AVs, along with the verification of each isolated fraction is assessed with several markers

The several fractions that derived from the AVs isolation method were identified by using various markers; Grp78-Bip (~63kD) was used as ER marker, LC3 as autophagosomal marker and p62 as a substrate of AVs [To this figure, Emmanouela Kallergi, PhD has also contributed to].

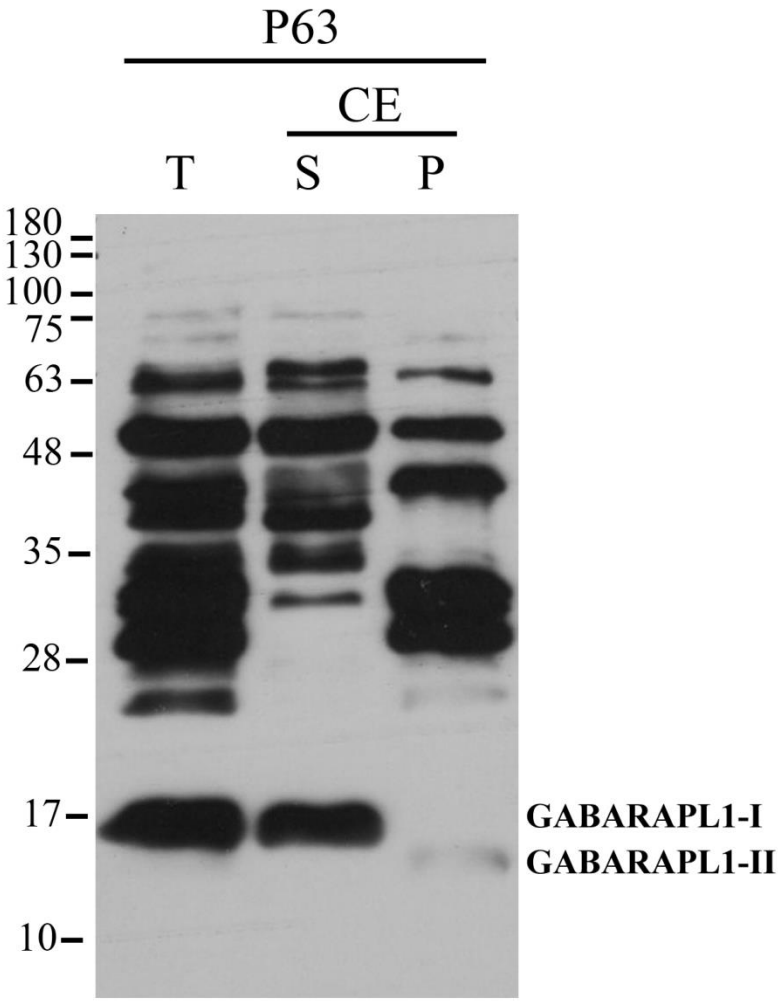

Figure S8 GABARAPL1 protein is present in the membrane of AVs

Isolated AVs from P63 male animals, were carbonate extracted and immunobloted against GABARAPL1. The GABARAPL1 antibody recognizes two bands: an upper band of approximately 17 kD corresponding to GABARAPL1-I and a lower band of 14 kD corresponding to the lipidated GABARAPL1-II, the species that is incorporated in autophagosomes.GABARAPL1-II is present only in the (P) of the AVs.